CHAPTER 11

Electro- and Photocatalytic Reduction of CO_2: The Homogeneous and Heterogeneous Worlds Collide?

DAVID BOSTON, KAI-LING HUANG, NORMA DE TACCONI, NOSEUNG MYUNG, FREDERICK MACDONELL AND KRISHNAN RAJESHWAR*

Department of Chemistry and Biochemistry, University of Texas at Arlington, Arlington Texas 76019-0065, USA
*Email: rajeshwar@uta.edu

11.1 Introduction and Scope

The catalytic reduction of carbon dioxide (CO_2) to fuels and organic compounds using light, electricity, or a combination of both, is not a new topic. References to this topic date back to the 1800s,[1–3] although rapid progress was made only since the 1970s. As elaborated below, a major challenge relates to the fact that the CO_2 molecule is extremely stable and is kinetically inert. A number of review articles and book chapters already summarize what has been accomplished on this challenging R&D topic.[4–14] This chapter contains an overview of recent developments in molecular catalysts for CO_2 reduction, summarized in Table 11.1 and Table 11.2, as well as a review of the progress made in our own laboratories against the backdrop of the rather vast body of

RSC Energy and Environment Series No. 9
Photoelectrochemical Water Splitting: Materials, Processes and Architectures
Edited by Hans-Joachim Lewerenz and Laurence Peter

Published by the Royal Society of Chemistry, www.rsc.org

Table 11.1 Electrochemical systems for CO_2 reduction with reduction potentials, electrolyte, electrodes, electrolysis potentials with all potentials are reported in NHE except where noted. (2-m-8-Hq = 2-methyl-8-hydroxyquinoline, 2-Qui. = 2-quinoxalinol, Hiq = Hydroxyisoquinoline, 4-m-1,10-Phen = 4-methyl-1,10-phenanthroline, dmbpy = 4,4′-dimethyl-2,2′-bipyridyl, phen = 1,10-phenanthroline, bpy = 2,2′-bipyridine, salophen = (4-acetamidophenyl) 2-hydroxybenzoate, dophen = 2,9-bis(2-hydroxyphenyl)-1,10-phenanthroline, tpy = 2,2′;6′,2″-terpyridine, TPP = 5,10,15,20-Tetraphenylporphin, N-MeIm = 1-methyl-imidazole, tBu-bpy = 4,4′-tertbutyl-2,2′-bipyridine, dppm = 1,1-Bis(diphenylphosphino)methane, dppe = 1,1-Bis(diphenylphosphino)ethane, dmg = dimethylglyoxime, cyclam = 1,4,8,11-tetraazacyclotetradecane, COD = 1,5-Cyclooctadiene, tmdnTAA = 5,7,12,14-tetramethyldinaphtho[b,i][1,4,8,11]tetraaza[14]annulene, HACD = 1,3,6,9,11,14-hexaazacyclohexadecane, decyclam = 1,8-diethyl-1,3,6,8,10,13-hexaazacyclotetradecane, TBA = tetra-N-butylammonium, TEtA = tetra-N-ethylammonium, TMA = tetra-N-methylammonium).

	Catalyst	*WE*	*Electrolyte*	*Solvent*	*Product*	*Efficiency*	*Redox Couple*	*CO_2 reduction*	*pH*	*Temp*	*Notes*	*Refs.*
1	$[Co(salophen)]^{2+}$	Hg	$Li(ClO_4)$	MeCN	CO, CO_3^{2-}		−1.02 V	−1.29 V			TON >20	23, 115, 116
2	$[Fe^{3+}(dophen)Cl]_2$	GC	$TBAPF_6$	DMSO	CO, $HCOO^-$, $C_2O_4^{2-}$	18.5%/ 67.2%/ 9.8%	−1.75 V	−1.69 V			improved by Li^+ and CF_3CH_2OH	117
3	$[Fe^{3+}(dophen)(N\text{-}MeIm)_2]_2$	GC	$TBAPF_6$	DMSO	CO, $HCOO^-$, $C_2O_4^{2-}$	13.3%/ 73.6%/ 7.3%	−1.72 V	−1.69 V			improved by Li^+ and CF_3CH_2OH	117
4	$[Fe^{3+}(dophen)Cl]_2$	GC	$TBAPF_6$	DMF	CO, $HCOO^-$, $C_2O_4^{2-}$	22.5%/ 57.2%/ 13.4%	−1.71 V	−1.69 V			improved by Li^+ and CF_3CH_2OH	117
5	$[Fe^{3+}(dophen)(N\text{-}MeIm)_2]_2$	GC	$TBAPF_6$	DMF	CO, $HCOO^-$, $C_2O_4^{2-}$	23.9%/ 58.9%/ 11.1%	−1.72 V	−1.69 V			improved by Li^+ and CF_3CH_2OH	117
6	$[Ni(cyclam)]^{2+}$	Hg	KNO_3	H_2O	CO	99%	−1.33 V	−1.0 V	4.10		4 h, 18 TOF/77.5 TON	118–121
7	$[Ni(tmdnTAA)]^{2+}$	GC	$TEtA(ClO_4)$	DMF:H_2O 1 : 1	CO		−0.84 V	−1.60 V				122
8	$[Ni(HACD)]^{2+}$	Hg (HMD)	$Li(ClO_4)$	H_2O	CO		−1.12 V	−1.36 V				123
9	$[Ni(decyclam)]^{2+}$	Hg (HMD)	$Li(ClO_4)$	H_2O	CO, $HCOO^-$, H_2		−1.23 V	−1.36 V	5.00			124

10	[CHx(Ni(cyclam))2]	HMD	$TBAPF_6$	MeCN/ H_2O	CO,H_2		–1.21 V	–1.46 V				125
11	$Co(dmg)_2(H_2O)Py$	GC	TMACl	EtOH	CO			–0.65 V		20–22 C		126
12	[Co(TPP)]	GC/Pt	TBAF	DMF	$HCOO^-$	10%	–0.53 V	–1.26 V				84, 127–129
13	[Fe(TPP)]	Hg	$TEtA(ClO_4)$	DMF	CO	94%	–1.41 V	–1.46 V			Mg^{2+}, or CF_3CH_2OH	130–134
14	$[Co(tpy)_2]^{2+}$	GC	$TBA(ClO_4)$	DMF	HCOOH		–1.46 V	–1.46 V			detected by chromotropic assay	135
15	$[Ni(tpy)_2]^{2+}$	GC	$TBA(ClO_4)$	DMF			–0.96 V	–0.96 V				135, 136
16	$[Ni(bpy)_3]^{2+}$	GC	$TBA(ClO_4)$	MeCN	CO, CO_3^{2-}		–0.9 V	–0.90 V				137
17	$[Ru(bpy)_2(CO)_2]^{2+}$	Hg (HMD)	$TBA(ClO_4)$	H_2O:DMF 9:1	$HCOO^-$, CO	34%/	–0.79 V	–1.26 V	9.5/6	30 C	16 TON/12 TON	37, 138
18	$[Ru(bpy)_2(CO)_2]^{2+}$	Hg	$TBA(ClO_4)$	MeOH	$HCOO^-$, CO, H_2	52.5%/ 32.0%	–0.79 V	–1.26 V				35, 38, 138
19	$[Ru(bpy)_2(CO)_2]^{2+}$	Hg	$TBA(ClO_4)$	MeCN	$HCOO^-$, CO, H_2	84.2%/ 2.4%/ 6.8%	–0.79 V	–1.06 V			$Me_2NH \cdot HCl$, Effiecency of $HCOO^-$ increases with increasing pk_a	35, 38, 43, 138
20	$[Ru(dmbpy)(bpy)(CO)_2]^{2+}$	Hg	$TBA(ClO_4)$	MeCN:H_2O 4:1	CO	71.80%	–0.89 V	–1.06 V				35
21	$[Ru(dmbpy)(bpy)(CO)_2]^{2+}$	Hg	$TBA(ClO_4)$	MeOH	CO, $HCOO^-$	34.2%/ 39.8%	–0.89 V	–1.06 V				35
22	$[Ru(dmbpy)_2(CO)_2]^{2+}$	Hg	$TBA(ClO_4)$	MeCN:H_2O 4:1	CO	65.30%	–0.89 V	–1.06 V				35
23	$[Ru(dmbpy)_2(CO)_2]^{2+}$	Hg	$TBA(ClO_4)$	MeOH	CO, $HCOO^-$	44.7%/ 32.5%	–0.89 V	–1.06 V				35
24	$[Ru(phen)_2(CO)_2]^{2+}$	Hg	$TBA(ClO_4)$	MeCN:H_2O 4:1	CO	61.5	-0.82 V	–1.06 V				35
25	$[Ru(phen)_2(CO)_2]^{2+}$	Hg	$TBA(ClO_4)$	MeOH	CO, $HCOO^-$	34.7%/ 24.5%	–0.82 V	–1.06 V				35
26	$[Ru(bpy)(Cl)_2(CO)_2]^{2+}$	Hg	$TBA(ClO_4)$	MeCN:H_2O 4:1	CO	87.80%		–1.06 V				35
27	$[Ru(bpy)(Cl)_2(CO)_2]^{2+}$	Hg	$TBA(ClO_4)$	MeOH	CO, $HCOO^-$	27.3%/ 37.7%		–1.06 V				35

Table 11.1 (*Continued*)

	Catalyst	*WE*	*Electrolyte*	*Solvent*	*Product*	*Efficiency*	*Redox Couple*	*CO_2 reduction*	*pH*	*Temp*	*Notes*	*Refs.*
28	$[Ru(dmbpy)(Cl)_2(CO)_2]^{2+}$	Hg	$TBA(ClO_4)$	MeCN:H_2O 4:1	CO	66.00%		–1.06 V				35
29	$[Ru(dmbpy)(Cl)_2(CO)_2]^{2+}$	Hg	$TBA(ClO_4)$	MeOH	CO, $HCOO^-$	39.2%/ 26.8%		–1.06 V				35
30	cis-$[Os(bpy)_2H(CO)]^+$	Pt_{mesh}	$TBAPF_6$	MeCN	CO	90%	–1.10, –1.36 V	–1.16 to –1.36 V				44
31	cis-$[Os(bpy)_2H(CO)]^+$	Pt	$TBAPF_6$	MeCN 0.3M H_2O	CO, $HCOO^-$	x/25%						44
32	$[Re(CO)_3(Cl)(bpy)]$	GC/Pt	TEtACl	DMF 10% H_2O	CO	98%	–1.47 V	–1.25 V				27, 29, 139
33	$[Re(CO)_3(ClO_4)(bpy)]$	GC	$TBAPF_6$	DMF 10% H_2O	CO	99%	–1.12 V	–1.25 V				26, 27, 29, 64
34	$[Re(CO)_3Cl(dmbpy)]$	GC	$TEtA(BF_4)$	MeCN	CO		–1.30 V	–1.52 V				28, 30
35	$[Re(CO)_3Cl(pbmbpy)]$	Pt_{mod}	$TBA(ClO_4)$	MeCN	CO, CO_3^{2-}	81%	–1.72 V *vs.* Ag/ 10 mM Ag^+	–1.85 V *vs.* Ag/ 10 mM Ag^+			14% oxalate	140
36	Re(tBu-bpy)$(CO)_3Cl$	GC	$TBAPF_6$	MeCN	CO	99%	–1.59 V	–1.76 V				28
37	$[Rh(COD)(bpy)]^+$	Pt		MeCN	CO, $HCOO^-$							141
38	$[(\eta^6\text{-}C_6H_6)Ru(bpy)Cl]^+$	Pt		MeCN	CO, $HCOO^-$							141
39	cis-$[Rh(bpy)_2(CF_3SO_3)_2]^+$	Pt	$TBAPF_6$	MeCN	$HCOO^-$		–0.98, –1.27 V				40 to 100 minute run, 12.3 TON	141, 142
40	cis-$[Ir(bpy)_2(CF_3SO_3)_2]^+$	Pt	$TBAPF_6$	MeCN				–0.96 to –1.36 V				141, 142
41	$[Ni(MeCN)_4(PPh_3)]^{2+}$	GC	$TBA(ClO_4)$	MeCN	CO, CO_3^{2-}							137
42	$[Ni_3(\mu\text{-}CNMe)(\mu_3\text{-}I)\text{-}(dppm)_3]^+$	Hg	$NaPF_6$	THF	CO, CO_3^{2-}		–0.89 V	–0.89 V				143
43	$[Ru(terpy)(dppe)Cl]^+$	Pt		MeCN	CO, $HCOO^-$							141
44	[RhCl(dppe)]	Hg	$TEtA(ClO_4)$	MeCN	$HCOO^-$	42%	–1.52 V	–1.21 V	–1.52		MeCN proton source	144

45	$[Ir(CO)Cl(PPh_3)_2]$	Hg	$TBABF_4$	DMF 10% H_2O	CO		–1.70 V	–1.06 V	20 C	145
46	$[Pd(PPh_3)(PPh_3)]$	GC	$TEtA(BF_4)$	MeCN $+H^+$	CO, H_2		–0.33 V			146
47	$[Pd(PPh_3)(PEt_3)]$	GC	$TEtA(BF_4)$	MeCN $+H^+$	CO, H_2		–0.69 V			146
48	$[Pd(PPh_3)(P(OMe)_3)]$	GC	$TEtA(BF_4)$	MeCN $+H^+$	CO, H_2		0.37 V			146
49	$[Pd(PPh_3)(P(CH_2OH)_3)]$	GC	$TEtA(BF_4)$	MeCN $+H^+$	CO, H_2		–0.51 V			146
50	$[Pd(PPh_3)(MeCN)]$	GC	$TEtA(BF_4)$	MeCN $+H^+$	CO, H_2		–0.48 V			146
51	$[Pd(PPh_3)_2(2\text{-m-}8\text{-Hq})]Cl$	Pt	$TBAPF_6$	MeCN	CO	60.2%		–0.94 V		147
52	$[Pd(PPh_3)_2(2\text{-m-}8\text{-Hq})]Cl$	Pt	$TBAPF_6$	MeCN:H_2O 25:2	CO, $HCOO^-$	25.2%/ 44.8%		–0.94 V		147
53	$[Pd(PPh_3)_2(2\text{-Qui})]Cl$	Pt	$TBAPF_6$	MeCN	CO	56.7%		–0.94 V		147
54	$[Pd(PPh_3)_2(2\text{-Qui})]Cl$	Pt	$TBAPF_6$	MeCN:H_2O 25:2	CO, $HCOO^-$	24.0%/ 37.7%		–0.94 V		147
55	$[Pd(PPh_3)_2(3\text{-Hiq})]Cl$	Pt	$TBAPF_6$	MeCN	CO	73%		–0.94 V		147
56	$[Pd(PPh_3)_2(3\text{-Hiq})]Cl$	Pt	$TBAPF_6$	MeCN:H_2O 25:2	CO, $HCOO^-$	31.7%/ 25.2%		–0.94 V		147
57	$[Pd(PPh_3)_2(1\text{-Hiq})]Cl$	Pt	$TBAPF_6$	MeCN	CO	74.5%		–0.94 V		147
58	$[Pd(PPh_3)_2(1\text{-Hiq})]Cl$	Pt	$TBAPF_6$	MeCN:H_2O 25:2	CO, $HCOO^-$	31.1%/ 25.8%		–0.94 V		147
59	$[Pd(PPh_3)_2(2\text{-m-}1,10\text{-phen})](ClO_4)_2$	Pt	$TBAPF_6$	MeCN	CO	60.9%		–0.94 V		147
60	$[Pd(PPh_3)_2(2\text{-m-}1,10\text{-phen})](ClO_4)_2$	Pt	$TBAPF_6$	MeCN:H_2O 25:2	CO, $HCOO^-$	31.5%/ 39.5%		–0.94 V		147
61	$[Pd(PPh_3)_2(dmbpy)](ClO_4)_2$	Pt	$TBAPF_6$	MeCN	CO	81.0%		–0.94 V		147
62	$[Pd(PPh_3)_2(dmbpy)](ClO_4)_2$	Pt	$TBAPF_6$	MeCN:H_2O 25:2	CO, $HCOO^-$	44.2%/ 30.0%		–0.94 V		147
63	$[Co(PPh_3)_2(2\text{-m-}1,10\text{-phen})](ClO_4)_2$	Pt	$TBAPF_6$	MeCN	CO	62.6%		–0.94 V		147
64	$[Co(PPh_3)_2(2\text{-m-}1,10\text{-phen})](ClO_4)_2$	Pt	$TBAPF_6$	MeCN:H_2O 25:2	CO, $HCOO^-$	32.6%/ 41.0%		–0.94 V		147
65	$[Co(PPh_3)_2(dmbpy)](ClO_4)_2$	Pt	$TBAPF_6$	MeCN	CO	83.4%		–0.94 V		147
66	$[Co(PPh_3)_2(dmbpy)](ClO_4)_2$	Pt	$TBAPF_6$					–0.94 V		147

Table 11.1 (*Continued*)

	Catalyst	*WE*	*Electrolyte*	*Solvent*	*Product*	*Efficiency*	*Redox Couple*	*CO_2 reduction*	*pH*	*Temp*	*Notes*	*Refs.*
				MeCN:H_2O 25:2	CO, $HCOO^-$	44.8%/ 29.1%						
67	$[Co(PPh_3)_2(2\text{-m-}8\text{-Hq})]Br$	Pt	$TBAPF_6$	MeCN	CO	61.4%		–0.94 V				147
68	$[Co(PPh_3)_2(2\text{-m-}8\text{-Hq})]Br$	Pt	$TBAPF_6$	MeCN:H_2O 25:2	CO, $HCOO^-$	25.8%/ 43.9%		–0.94 V				147
69	$[Rh_2(PhCHOHCOO)_2(phen)_2(H_2O)_2]^{2+}$	Pt	$TBA(BF_4)$	DMF:H_2O 10:1	CO, $HCOO^-$	85-90%	–0.55 V	–0.74 V				148
70	$[Fe_4S_4(SCH_2Ph)_4]^{2-}$	Hg	$TBA(BF_4)$	DMF	$HCOO^-$			–1.76 V				149
71	$[Fe_4S_4(SXN^-)_4]^{2-}$	Hg	$TBA(BF_4)$	DMF	$HCOO^-$	40% / 23%		–1.80 V			$X = -COCMe^{2-}$, $COC_6H_4CH_2$	150
72	Pyridine	Pt/Pd/p-GaP	$Na(ClO_4)$	H_2O	HCOOH, MeOH	10.8%/ 22%	–0.34 V		5.00		30–50 μA	25, 110, 114

Table 11.2 Photochemical systems for CO_2 reductions with reaction conditions, catalysts, chromophore, and products(tb-cabinol = tris(4′-methyl-2,2′-bipyridyl-4-methyl)carbinol, dmb = 4,4′-dimethyl-2,2′-bipyridyl, TEA = triethylamine, TEOA = triethanolamine, BNAH = 1-Benzyl-1,4-dihydronicotinamide, H_2A = Ascorbic Acid, bpz = 2,2′-bipyrazine, HMD = 5,7,7,12,14,14-hexamethyl-1,4,8,11-tetraazacyclotetradeca-4,11-diene, cyclam = 1,4,8,11-tetraazacyclotetradecane, pr-cyclam = 6-((p-methoxybenzyl)pyridin-4-yl)methyl-1,4,8,11 -tetraazacyclotetradecan, MV = methyl viologen, phen = 1,10-phenanthroline bpy = 2,2′-bipyridine, EDTA = ethylenediaminetetraacetate, TPA = tripropylamine, TMA = trimethylamine, TPP = 5,10,15,20-Tetraphenylporphin, TBtA = tributylamine, TPtA = tripentylamine, TiBA = triisobutylamine, TMEDA = N,N,N,N-tetramethylethylenediamine, {[Zn(TPP)]/[$Re(CO)_3$(pic)(bpy)]} = 5-[4-[(2-methoxy-4-([rhenium (I) tricarbonyl (3-picoline)]4-methyl-2,2′-bipyridine-4′-carboxyamidyl) carboxyamidyl) phenyl] phenyl]-10,15,20-triphenyl porphyrinatozinc(II)).

	Chromophore	*Cat/Relay*	*Donor*	*Solvent*	*Product*	ϕ*(mol/einsteins)*	*TON/TOF*	*pH*	*irradiation time*	*λ/nm*	*Refs.*
1	$Ru(bpy)_3^{2+}$		TEOA	15%H_2O in DMF	$HCOO^-$	0.049	19/9.5				151
2	$Ru(bpy)_3^{2+}$		TEOA	15%H_2O in DMF	$HCOO^-$	0.096	43/21.5				151
3	$Ru(bpy)_3^{2+}$	MV^{2+}	TEOA. EDTA	H_2O	$HCOO^-$	0.01	75/18.8		4 hr		152
4	$Ru(bpy)_3^{2+}$	Co^{2+}/bpy	TEA, TPA, TEOA, TMA	MeCN/donor/H_2O, 3:1:1 (vol/vol)	CO, H_2		9/0.4		22 hr		153
5	$Ru(bpy)_3^{2+}$	Co^{2+}/2,9-Me_2phen	TEA, TPA, TMA, TBA, TPtA, TiBA, TMEDA	MeCN or DMF/donor/H_2O, 3:1:1 (vol/vol), DMF/ H_2O 3:2	CO, H_2	0.012 (CO), 0.065 (H_2)		8.6	26 hr		154
6	$Ru(bpy)_3^{2+}$	$Ru(bpy)_2(CO)_2^{2+}$	TEOA	H_2O /DMF 1:9 and DMF	$HCOO^-$	2% , 1%		6/9.5	10 hr		41, 42, 138
7	$Ru(bpy)_3^{2+}$	$Ru(bpy)_2(CO)_2^{2+}$	BNAH	H_2O /DMF 1:9	$HCOO^-$, CO	0.03 ($HCOO^-$), 0.15 (CO)	50, 125	6/9.5	10 hr		41, 42, 138
8	$Ru(bpy)_3^{2+}$	$Ru(bpy)_2(CO)H^+$	TEOA		$HCOO^-$	0.15	161/80.5				151
9	$Ru(bpy)_3^{2+}$	$Ru(bpy)_2(CO)X^{n+}$	TEOA		$HCOO^-$		163/81.5 (X = Cl) 54/27 (X = CO)				151
10	$Ru(bpy)_3^{2+}$	$Co(HMD)^{2+}$	H_2A		CO, H_2						77

Table 11.2 (*Continued*)

	Chromophore	*Cat/Relay*	*Donor*	*Solvent*	*Product*	*ϕ(mol/einsteins)*	*TON/TOF*	*pH*	*irradiation time*	*λ/nm*	*Refs.*
11	$Ru(bpy)_3^{2+}$	$Ni(cyclam)^{2+}$	H_2A	H_2O	CO, H_2	0.001 (CO)		4	22 hr		76, 78
12	$Ru(bpy)_3^{2+}$	$Ni(Pr\text{-}cyclam)^{2+}$	H_2A	H_2O	CO, H_2		ca. 0.005 (CO)	5.1	4 hr		79
13	$Ru(bpy)_3^{2+}$	$Bipyridinium^+$, Ru/OS Colloid	TEOA	H_2O	CH_4, H_2	10^{-4} (CH_4), 10^{-3}(H_2)		7.8	2 hr		87
14	$Ru(phen)_3^{2+}$	$Ni(cyclam)^{2+}$	H_2A	H_2O	CO, H_2		< 0.1	4	22 hr		78
15	$Ru(phen)_3^{2+}$	Pyridine	H_2A	H_2O	CH_3OH	7.22×10^{-7}	0.9	5	6 hr	470	86
16	$Ru(bpz)_3^{2+}$	Ru colloid	TEOA	H_2O/EtOH 2:1	CH_4	0.04%	15	9.5	2 hr		87, 88
17	$Ru(dmb)_3^{2+}$	$ReCl(dmb)(CO)_3$	BNAH	DMF:TEOA 5:1	CO	0.062	101/6.3		16 hr	≥500	69
18	$[Ru(phen)_2\text{-}(phenC_1cyclam)Ni]^{2+}$		H2A	H_2O	CO, H_2		< 0.1	5.1	4 hr		79
19	$[(dmb)_2Ru(MebpyC_3OHMebpy)\text{-}Re(CO)_3Cl]^{2+}$		BNAH	DMF:TEOA 5:1	CO	0.12	170/10.7		16 hr	≥500	69
20	$[(dmb)_2Ru(MebpyC_nH_{2n}Mebpy)\text{-}Re(CO)_3Cl]^{2+}$		BNAH	DMF:TEOA 5:1	CO	0.13 (n = 2), 0.11 (n = 4,6)	180/15 (n − 2), 120/10 (n = 4,6)		16 hr	<500	73
21	$[(dmb)_2Ru(MebpyC_3OHMebpy)\text{-}Re(CO)_3\{P(POEt)_3\}]^{3+}$		BNAH		CO	0.21	232/19.3				70
22	$[Ru\{(MebpyC_3OHMebpy)\text{-}Re(CO)_3Cl\}_3]^{2+}$		BNAH	DMF:TEOA 5:1	CO	0.093	240/15		16 hr	≥500	69
23	$[(dmb)_2Ru(MebpyC_2Mebpy)\text{-}Re(CO)_2\{P(p\text{-}FPh)\}_2]^{2+}$		BNAH	DMF:TEOA 5:1	CO	0.15	207/281		20 hr	>500	74
24	$[(dmb)_2Ru(tb\text{-}carbinol)\{Re(CO)_3Cl\}_2]^{2+}$		BNAH	DMF:TEOA 5:1	CO		190/11.8		16 hr	≥500	71, 72
25	$[[(dmb)_2Ru]_2(tb\text{-}carbinol)Re(CO)_3Cl]^{2+}$		BNAH	DMF:TEOA 5:1	CO		110/6.9		16 hr	≥500	52,53
26	p-terphenyl	$Co(cyclam)^{3+}$	TEOA	MeOH/MeCN 1:4	CO, H_2, $HCOO^-$	0.25 ($CO + HCOO^-$)			1 hr	290	81
27	p-terphenyl	$Co(HMD)^{2+}$	TEOA	MeOH/MeCN	CO, H_2, $HCOO^-$				1 hr	313	81, 83
28	Phenazine	$Co(cyclam)^{3+}$	TEA	MeOH/MeCN/ TEA 10:1:0.5	CO, H_2, $HCOO^-$	0.07 ($HCOO^-$)			3 hr	313	82

29	Fe^{III}(TPP)		TEA	DMF	CO		70	180 hr	UV	85
30	Co^{III}(TPP)		TEA	MeCN	$HCOO^-$, CO		>300 (total)	200 hr	<320	84
31	{[Zn(TPP)]/ [Re(CO)$_3$(pic)(bpy)]}		TEOA	DMF:TEOA 5:1	CO		30		>520	155
32	[Re(4,4′-(MeO)$_2$-bpy)(CO)$_3$-(P(OEt)$_3$)]$^+$	[Re(bpy)(CO)$_3$-(CH$_3$CN)]$^+$	TEOA	DMF:TEOA 5:1	CO	0.59		25 hr	<330	65
33	ReCl(bpy)(CO)$_3$		TEOA	DMF:TEOA 5:1	CO		27	4 hr	>400	64
34	ReCl(bpy)(CO)$_3$		TEA	DMF:TEA 0.8 M TEA	CO		8.2(Cl) 42(COO)	25 hr		62
35	ReBr(bpy)(CO)$_3$		TEOA	TEOA:DMF 1:2	CO	0.15	20/5	11.7 min	436	57, 59, 64
36	ReOCHO(bpy)(CO)$_3$		TEOA	TEOA:DMF 1:5	CO	0.05	12	20 min	>330	64, 68
37	[Re(bpy)(CO)$_3$(PR$_3$)]$^+$		TEOA	DMF:TEOA 5:1	CO	0.38 (R = Oet), 0.013 (R = nBu), 0.024(R = Et), 0.2 (OiPr), 0.17 (R-Ome)	7.5/0.5 (R = Oet), <1/<0.1 (R = nBu), 6.2/0.5 (OiPr), 5.5/0.4 (R-Ome)	13 hr	365	66, 156
38	[Re(bpy)(CO)$_3$(P(Ohex)$_3$)]$^+$		TEA	CO_2(liquid)	CO		2.2/1.1	2 hr	365	157
39	[Re(bpy)(CO)$_3$(P(OiPr)$_3$)]$^+$		TEOA	DMF:TEOA	CO		15.6/0.7	24 hr	365	158
40	[Re(bpy)(CO)$_3$(4-X-py)]$^+$		TEOA	TEOA:DMF 1:5	CO	0.03 (x = tBu, Me,H), 0.04 (x = C(O)Me), 0.13 (X = CN)	1/0.1 (x = tBu, Me,H, C(O)Me), 3.5/0.4 (X = CN)	8.5 hr	365	159
41	[Re(4,4′-(CF$_3$)$_2$-bpy)(CO)$_3$(P(OEt)$_3$)]$^+$		TEOA	DMF:TEOA 5:1	CO	0.005	<1/<0.1	17 hr	365	156
42	[Re(dmb)(CO)$_3$(P(OEt)$_3$)]$^+$		TEOA	DMF:TEOA 5:1	CO	0.18	4.1/0.2	17 hr	365	156
42										

literature. Similar compilations for semiconductor-based studies appear in reference 5 and other sources cited above. The focus here is on the use of inorganic molecules and/or semiconductor electrode materials to sustain the reduction of CO_2. Biochemical or bioelectrochemical approaches (for example, see reference 10), which are clearly of interest and importance from a comparative perspective of the artificial photosynthesis approach under discussion, are not addressed specifically.

At the outset it seems prudent to review critically the various terminologies used in the literature, in order to place the present discussion in the proper context. Thus a *homogeneous* CO_2 reduction system consists of an assembly of dissolved (molecular) catalyst that may be present in addition to a light absorber, sacrificial electron donor, and/or electron relay all in the same solution. In some cases, the light-absorbing function may be built into the same catalyst molecule, but the key is that all participating components are present in the same phase. A *heterogeneous* system, on the other hand, has the catalyst present in a different (*i.e*. solid) phase. The catalyst may be a metal that is anchored to a support, which in turn may also be a metal or an inorganic semiconductor. We believe that this distinction based on phase is less important (and may even be misleading) when applied to a situation such as CO_2 reduction; thus this terminology is avoided in the discussion that follows. The terminology problem is illustrated by approaches based on the tethering (or strong adsorption) of (catalyst) *molecules* on metal or semiconductor electrode surfaces. Does the CO_2 reduction occur in such cases in the solution phase or at the solid/liquid phase boundary? Clearly the distinction between ''homogeneous'' and ''heterogeneous'' becomes much fuzzier here.

The term ''photoelectrochemical'' has been largely applied in the literature to situations involving a semiconductor electrode, whereas we apply this terminology in the present context to denote situations involving either the traditional semiconductor/liquid junctions or catalyst molecules that serve the dual functions of both light absorption and electron transfer mediation. Alternate descriptions based on ''electrocatalytic'' and ''photocatalytic'' systems are synonymous and denote approaches wherein the CO_2 reduction is driven electrochemically and with the assistance of light, respectively. On the other hand, the concept of *photochemical* systems is best reserved for approaches based on colloidal suspensions of metal or inorganic semiconductor nanoparticles or purely homogeneous systems with molecular catalysts in solution. While approaches using colloids or nanoparticles have been reviewed[6] (and indeed one example of it is discussed below), we believe that they are problematic in terms of process scale-up and product separation. Systems based on colloidal suspensions also are prone to low conversion efficiencies stemming largely from the prevalence of back reactions. These issues are largely circumvented in *photoelectrocatalytic* systems, in whcih the colloidal particles are anchored onto a solid electronically conducting support (*e.g*. conducting transparent glass) so that a negative electrode potential can be applied to bias forward electron transfer and thus inhibit the back recombination pathway.

11.2 Thermodynamics of CO_2 Reduction

Equations (11.1) to (11.6), below show the various products resulting from the reduction of CO_2, ranging from a one-electron reduction to the radical anion all the way to an 8-electron deep reduction to methane. Multiple proton-coupled electron transfer (PCET) steps occur in Equations (11.2) to (11.6), and herein lies the rich electrochemistry inherent with this system. Given that these electrochemical processes are pH-dependent, the potentials below are given at pH 7 in aqueous solution versus the normal hydrogen electrode (NHE), 25 °C, 1 atm gas pressure, and 1M for the solutes.[5,15]

$$CO_2 + e^- \rightarrow CO_2^{\bullet -} \qquad E^\circ = -1.90V \qquad (11.1)$$

$$CO_2 + 2e^- + 2H^+ \rightarrow CO + H_2O \qquad E^\circ = -0.53V \qquad (11.2)$$

$$CO_2 + 2e^- + 2H^+ \rightarrow HCOOH \qquad E^\circ = -0.61V \qquad (11.3)$$

$$CO_2 + 4e^- + 4H^+ \rightarrow H_2CO + H_2O \qquad E^\circ = -0.48V \qquad (11.4)$$

$$CO_2 + 6e^- + 6H^+ \rightarrow H_3COH + H_2O \qquad E^\circ = -0.38V \qquad (11.5)$$

$$CO_2 + 8e^- + 8H^+ \rightarrow CH_4 \qquad E^\circ = -0.24V \qquad (11.6)$$

While progress on the concerted $2e^- - 2H^+$ reduction to CO or formate has been impressive (see below), the formation of more useful fuel products such as methanol and methane necessitates multiple electron and proton transfers. The kinetic barriers associated with these are formidable, as briefly discussed next.

11.3 Energetics of CO_2 Reduction

11.3.1 General Remarks

The terms ‘‘electrocatalytic‘‘ and ‘‘photocatalytic’’ are used herein in a generic sense with the implicit and important recognition that the reactions above are endergonic with ΔG values ranging from 1.90 eV to 8.31 eV respectively. Putting an electron into the linear and inert CO_2 molecule (Reaction (11.1)) entails a steep energy cost because of the resultant structural distortion.[8] This is reflected in the very negative reduction potential for Reaction (11.1) above. Thus this radical formation step is very energy-inefficient and the steep activation barrier associated with it, must be avoided *via* the use of a catalyst.[16,17] From an electrochemical perspective, this translates to sizeable ‘‘overpotentials’’ (spanning several hundred mV) for driving this reduction process.[16,17] Thus a catalyst molecule, by interacting strongly with the radical anion, can reduce this energy barrier. This is the essence of many of the catalysis-based approaches to be discussed below.

11.3.2 Band Energy Positions of Selected Oxide Semiconductors and CO_2 Redox Potentials

In a discussion of the energetics of CO_2 photoreduction, it is convenient to display the relevant solution redox potentials in an energy diagram on the same scale as the semiconductor band-edges. The latter are experimentally derived from flat-band potential measurements.[18] Figure 11.1 shows an example of this diagram for several inorganic oxide semiconductors. As with solution redox couples involving proton transfer, the oxide band-edges are pH-dependent, shifting at a Nernstian rate of −59 mV/pH unit at 25 °C. Therefore, the particular situation illustrated in Figure 11.1 pertains to a solution pH of 7. A similar diagram appears in reference [5] for TiO_2, Cu_2O, and eight other non-oxide semiconductors (see Figure 11.4 therein).

Such a representation is useful for assessing whether the photogenerated carriers in the semiconductor are thermodynamically capable of reducing (or oxidizing) a given species in the solution phase. We assume at the outset that these carriers are thermalized such that they possess average energies close to the semiconductor band edges. A further assumption is that Fermi level pinning does not occur, so that the band-edges are fixed relative to the energies of solution redox couples.[18] Therefore, any reduction reaction whose potential

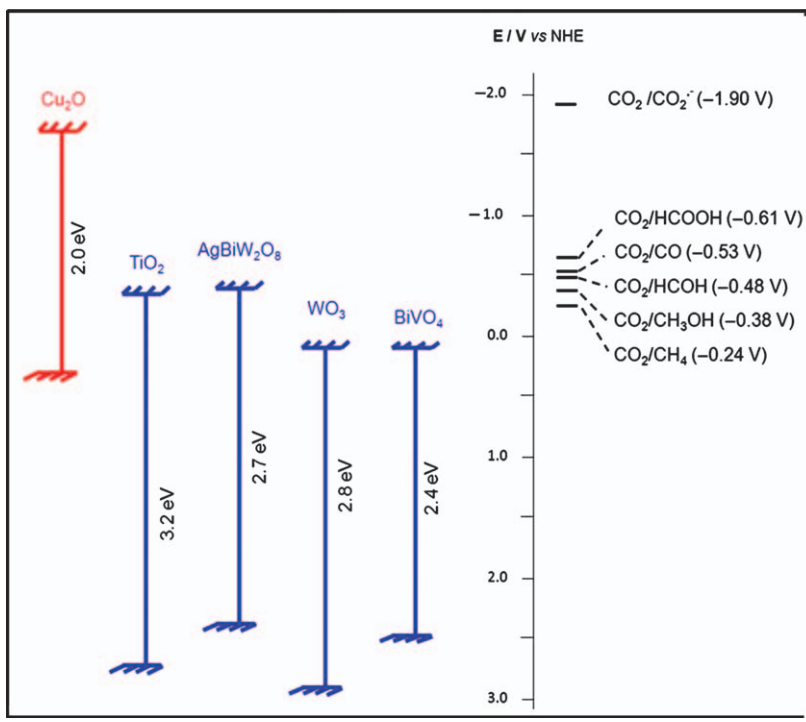

Figure 11.1 Comparison between the band-edges of selected semiconductors and relevant thermodynamic potentials for CO_2 reduction. All data are for pH 7 and versus a normal hydrogen electrode (NHE).

falls above the conduction band-edge (for a given semiconductor) would be thermodynamically prohibited because the photogenerated electrons would simply not have enough energy to sustain the reduction.

Given that the redox potentials for most of the CO_2-derived reduction processes lie negative of the hydrogen evolution reaction (HER) in water (the two exceptions being the deep reduction of CO_2 to methanol and methane), the more negative the conduction band-edge location is, the better is the corresponding semiconductor candidate. The thermodynamic driving force for the reduction is roughly given by the difference between the semiconductor conduction band-edge and the corresponding redox potential. Thus the more negative the semiconductor conduction band edge is, the greater the driving force (all other factors being equal). However, it is worth emphasizing that such thermodynamic arguments are only *starting points*. Whether the reduction occurs at a fast rate depends on the inherent kinetics at that semiconductor/solution interface and the associated overpotentials. It is clear from Figure 11.1 that the use of new-generation semiconductors such as $AgBiW_2O_8$ and even materials such as Cu_2O rather than the well-studied TiO_2 prototype may be advantageous because of the relatively negative location of their conduction band edges. Results on both these oxide semiconductors are presented below.

11.3.3 Molecular Orbital Energy Diagram for $Ru(phen)_3^{2+}$ Compared with CO_2 Redox Potentials

For photochemical reduction in homogeneous system, the chromophores $[Ru(phen)_3]^{2+}$ and $[Ru(bpy)_3]^{2+}$ still represent one of the most widely used systems for driving highly endogonic redox reactions, due to their excited state energetics and good chemical stability.[19] We make a particular point of introducing this chromophore as it has been the primary one used in our own studies on homogeneous photochemical reduction of CO_2. As shown schematically in Figure 11.2, the reduction potential for both the photoexcited state $[Ru(phen)_3]^{2+}*$ or the reductively quenched chromophore $[Ru(phen)_3]^{+}$ are negative of the key CO_2 reduction couples, meaning that these species are thermodynamically capable of reducing CO_2. The difficulty in using them is that they themselves lack the chemical functionality to lower the activation barriers involved and are only capable of delivering a single electron each towards these multi-electron reactions. It is also worth noting that the initial conversion of CO_2 to CO is the energy "hog" in the overall process and consumes a minimum of 1.33 eV.[20] Much of the progress associated with the conversion of CO_2 to CO and formate has revolved around electro- and photocatalytic strategies for minimizing the additional overpotential over and above this minimum threshold.

11.4 Electrocatalytic CO_2 Reduction with Molecular Catalysts

Many homogeneous catalysts have been developed for both electrochemical and photochemical systems; however, few are capable of deeper reduction than the

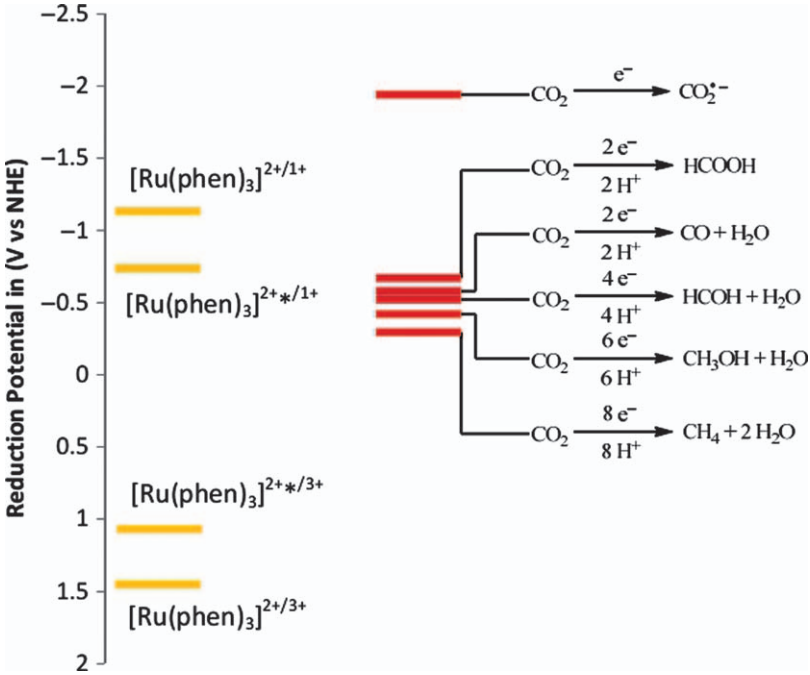

Figure 11.2 Reduction potentials of carbon dioxide reduction as compared with the HOMO and LUMO levels of $[Ru(phen)_3]^{2+}$.

two-electron reduced products of CO_2, such as CO and formic acid. Table 11.1 contains a collection of all (at least to the best of our knowledge) reported molecular electrocatalytic systems for CO_2 reduction in which the actual products of reduction were identified. The table includes information on the catalyst, electrochemical conditions, and products. Of the 72 entries in Table 11.1, 71 are metal complexes, and the final product represents a net two-electron reduction of CO_2. The sole organic entry (#72) is pyridine, and this simple catalyst is able to catalyze even deeper reduction to products including methanol as described in the next section. Metal phthalocyanines have also been reported to catalyze the even deeper reduction of CO_2 to CH_4, but these are known to form electrochemically active films and thus are more of a heterogeneous catalyst.[21]

11.4.1 Pyridine for Electrocatalytic Reduction of CO_2

Bocarsly *et al.* have shown it is possible to reduce CO_2 to methanol by using a very simple electrocatalyst, pyridinium, which upon reduction can bind CO_2 to form carbamate-type adducts and, *via* redox cycling, shuttles six electrons to ultimately form methanol, as shown in Figure 11.3.[22]

Through simulation of experimental results and kinetic studies, they were able to deduce the possible mechanism of the reduction of CO_2 to methanol.[23,24] The electron transfer in this process proceeds through an inner sphere electron

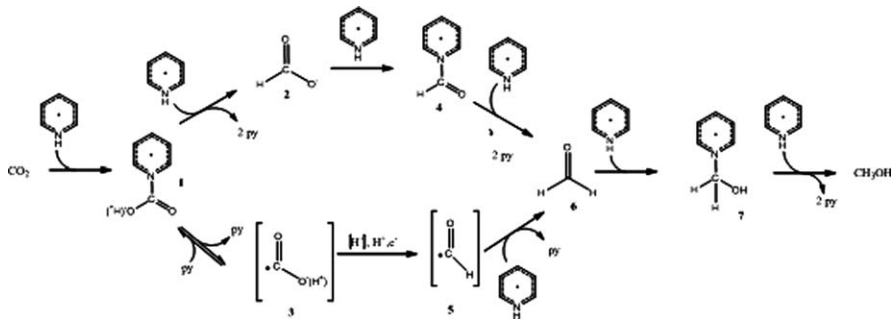

Figure 11.3 Pyridinium catalyzed reduction of CO_2.[3,25,114]

transfer as was shown by $^{13}C^{15}N$ coupling in NMR and by gas-phase photoelectron spectroscopy.[25] Based on the calculated bond distance and bond angles, the nature of the N-CO_2 bond was found to be primarily of π-character as opposed to σ-character. Reductions beyond the first electron transfer were found to depend on the electrodes being used.[25] For electrodes with low hydrogen overpotential, such as Pt or Pd, it was found that dissociation of the pyridine-formate radical adduct occurs, allowing the next reduction to formate or formic acid to take place on the electrode surface.[25] For electrodes with high hydrogen overpotential, the reaction is catalyzed entirely by the pyridinium with no dissociation of the formate radical, but a second pyridinium radical passes an electron to the pyridine-formate radical adduct instead.[24,25] With low hydrogen overpotential electrodes, formic acid adsorbs onto the surface to produce the hydroxyformyl radical that reacts with a surface hydrogen atom to make the formyl radical, which is reduced finally to the pyridinium radical to formaldehyde, as shown at the bottom of Figure 11.3.[25] For high hydrogen overpotential electrodes, formic acid reacts with the pyridinium radical to make the pyridinium-formyl adduct, which is reduced further by a second pyridinium radical to form free formaldehyde and two equivalents of pyridine, as shown at the top of Figure 11.3.[25] For both electrode types, the reduction of formaldehyde results from the reaction with a pyridinium radical to form a pyridinium-formyl radical adduct, and this species reacts with a second pyridinium to produce methanol and two equivalence of pyridine.[25] There is some debate about the mechanism proposed by Bocarsly *et al.*: some groups claim a non-innocent role of the surface in the process and thus a process which is necessarily heterogeneous.[23,25]

11.4.2 Rhenium Polypyridyl Complexes for Electrocatalytic Reduction of CO_2

The highly selective and efficient nature of the *fac*-Re(bpy)$(CO)_3$X (X = Cl, Br) has driven the large amount of research activity of this complex towards electrochemical CO_2 reduction.[13,15,26–32] The catalytic reduction can proceed through two different pathways: a one-electron or a two-electron pathway (Figure 11.4), both of which yield CO.[27] In the one-electron pathway

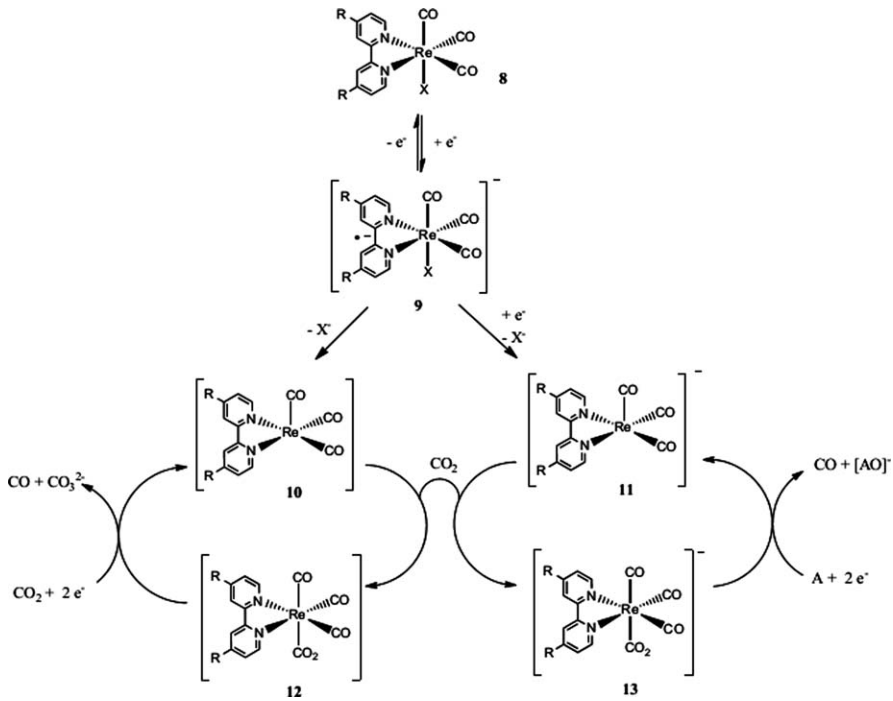

Figure 11.4 The proposed one-electron and two-electron pathways.

(Figure 11.4, left), the coordinatively unsaturated Re(0) species binds CO_2 to give the equivalent of a bound $CO_2^{\bullet -}$ radical anion, which upon reaction with another $CO_2^{\bullet -}$ radical anion (CO_2 and a second electron) disproportionates to yield CO and CO_3^{2-}.[33,34] In the two electron pathway (Figure 11.4, right), the starting complex is reduced twice, and following loss of the halide yields a coordinatively unsaturated Re(-1) complex. Binding of CO_2 and in the presence of some oxide acceptors, such as H^+, yields CO and H_2O.[13,27]

Both of these pathways, the one-electron and the two-electron, are accessible with the same complex but at different potentials. Based on the work published by Meyer *et al.*,[27] species **9**, the one-electron reduced species, is formed at -1.11 V versus NHE. Under Ar, this couple is also associated with the formation of a Re-Re dimer, [*fac*-Re(bpy)$(CO)_3]_2$, which has been implicated as the reactive species in some studies.[27,30] The second reduction of *fac*-[Re(bpy)-$(CO)_3$X]$^-$ is observed at –1.26 V *vs.* NHE and can also result in halide loss and generation of the active catalyst.[13] At a more negative potential of -1.56 V *vs.* NHE, the reaction proceeds through the two-electron reduction pathway as shown on the right side of Figure 11.4 to give CO without the formation of carbonate.[27] Studies by Kubiak *et al.*[28] have shown that by changing the 4,4′ substituents on the bpy-ligand in *fac*-Re(bpy)$(CO)_3$X it was possible to enhance the electrocatalysis reaction rate from 50 $M^{-1}s^{-1}$ for H to 1000 $M^{-1}s^{-1}$ for the *t*-Bu derivative as well as to increase the Faradaic efficiency ($\sim$99%).

11.4.3 Ruthenium Polypyridyl Complexes for Electrocatalytic Reduction of CO_2

Other than rhenium-based complexes, ruthenium polypyridyl complexes are the next most well explored. $Ru(phen)_2(CO)_2^{2+}$ and $Ru(bpy)_2(CO)_2^{2+}$ are reported to reduce CO_2 electrocatalytically. These complexes typically make CO, H_2, and formate as products of reduction,[35–42] with the ratio of these products being pH dependent.[39,40] At pH 6, the products are CO and H_2; however at pH 9.5, formate is produced in addition to CO and H_2.

Two different catalytic pathways have been proposed: the one proposed by Tanaka *et al.* is shown in Figure 11.5,[39,40,43] and the other proposed by Meyer *et al.*[9] is shown in Figure 11.6. Both schemes involve the reduction and loss of CO to form a neutral coordinatively unsaturated $Ru(L\text{-}L)_2(CO)$ (**16**) species. Tanaka *et al.* can start with the dicarbonyl, species **14**, or the monocarbonyl monochloride, species **15**,[39,40,43] where the electrons are thought to sit on the bpy ligands.[9] Tanaka *et al.* propose that **16** can react with either CO_2 or H^+ to form one of two intermediates, the formato species **17** or the hydride species **19**.[39,40,43] The species **17** reacts with a proton to form the metallo-carboxylic acid (species **18**), which at pH 6 and reforms the dicarbonyl complex **14** but at pH 9.5, adds two electrons to produce formate and **16**.[39,40,43] The generation of hydrogen is explained *via* the formation of the hydride in a competing side reaction.

As shown in Figure 11.6, Meyer *et al.* propose that the hydride species **19** is involved directly in the CO_2 fixing cycle and that – after reduction to **21** – insertion of CO_2 into the metal hydride bond forms the formato-complex (species **22**).[9,44–46] A further reduction step releases formate and generates a solvate complex, which reacts with water to reform the hydride **19**.[46] Although there is

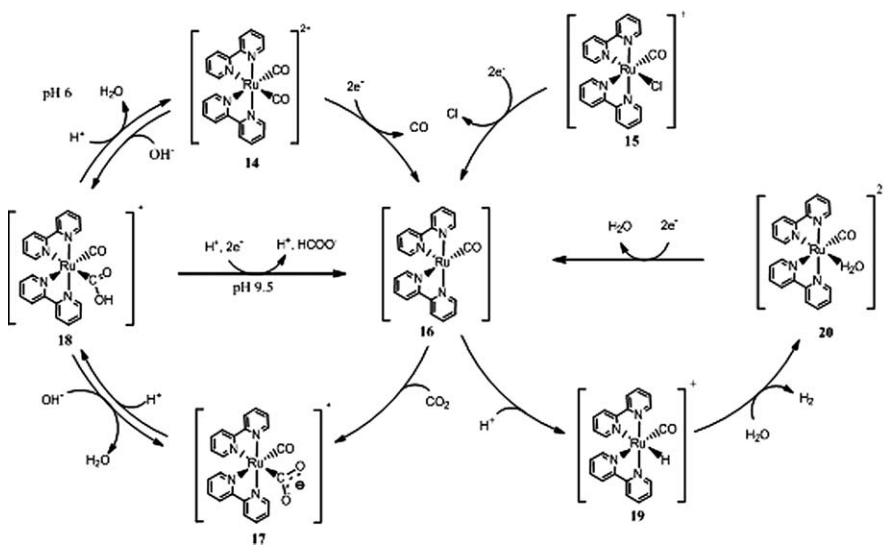

Figure 11.5 Electrocatalytic reduction of CO_2 by $[Ru(bpy)_2(CO)_2]^{2+}$ with possible pathways for CO, formate and H_2 formation.

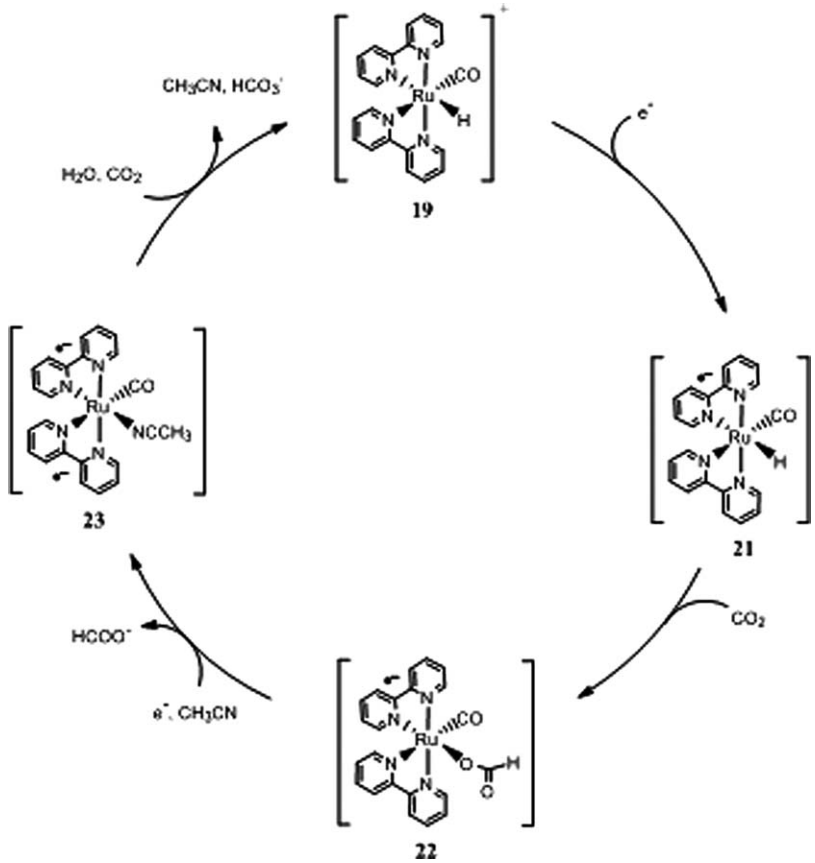

Figure 11.6 Electrochemical reduction of CO_2 *via* hydride bond insertion to form formate.

no direct evidence for the formation of species **23**, the catalysis could proceed through a process that goes directly from species **22** to species **19** with loss of formate and reduction of water in one step.[46]

11.5 Electrocatalytic Materials Inspired by Fuel Cell Electrode Nanocomposites

11.5.1 Pt-carbon Black-TiO_2 Nanocomposite Films Containing Highly Dispersed Pt Nanoparticles as Applied to CO_2 Electroreduction

The proton electrolyte membrane (PEM) fuel cell and water electrolysis technologies have obvious synergies, especially as they pertain to the proton exchange membrane (*e.g.* Nafion) separating the two compartments. Therefore, it is not surprising that the electrochemical engineering underpinning both these

technologies shares many common aspects.[19] It occurred to us that many of the design aspects related to fuel cell electrode materials are equally relevant to the CO_2 electroreduction system. This led us to evaluate the applicability of oxygen reduction reaction (ORR) cathode materials for the CO_2 electroreduction application.[47] For this purpose, we utilized a Pt-carbon black-TiO_2 nanocomposite film electrode in conjunction with a pyridinium ion co-catalyst.[47] The latter is further elaborated in the next section of this chapter.

The photocatalytic route for modifying a C-TiO_2 support with Pt (or another target metal or bimetallic Pt-Pd electrocatalyst) hinges on the fact that TiO_2 is a semiconductor and thus is capable of absorbing light of wavelengths equal to or greater than those corresponding to its band gap energy, E_g.[48,49] As elaborated elsewhere, this in situ catalyst photodeposition strategy first consisted of ultrasonically dispersing: (i) a suitable carbon black; (ii) the metal oxide (in desired proportions); (iii) the catalyst precursor salt (*e.g.* H_2PtCl_6, $PdCl_2$); (iv) an electron donor or hole scavenger (*e.g.* formate); and (v) a surfactant (as needed). This dispersion was introduced into a custom-built photochemical reactor[50] equipped with a medium pressure Hg arc lamp as a UV irradiation source. A crucial aspect of this synthetic approach is that photoinduced electron transfer from the TiO_2 phase to the carbon support results in the uniform deposition of the metal catalyst throughout the composite as a whole rather than localized deposition on the titania surface.[48,49]

For preparation of Pt-Pd/C-TiO_2, an essentially similar procedure was used, except for addition of the Pd precursor salt to the photocatalytic deposition medium. The two metals (Pt and Pd) were photodeposited sequentially, with the total loading of the noble metal in the nanocomposite being maintained the same in both cases. Other details may be found in refernces 48 and 49.[49,48]

Figure 11.7 contains representative high-resolution transmission electron micrographs of Pt/C-TiO_2 (Figure 11.7a) and Pt-Pd/C-TiO_2 (Figure 11.7b) nanocomposite powders. In both images, the dark spots are the metallic nanoclusters that are seen highly dispersed on the carbon-oxide support (showing corrugated appearance). Metal cluster sizes are seen to be in the range 3–5 nm, with slighter larger sizes and elongated shapes in the case of the Pd-Pt nanocomposite (Figure 11.7b). It is worth noting that photocatalytic deposition at a neat TiO_2 surface (*i.e.* without carbon black in electronic contact) affords Pt nanoparticles that are significantly larger than those obtained with the C-TiO_2 support.[49] Consistent with the essentially similar nanocomposite morphology in both cases, cathodes derived from either Pt/C-TiO_2 or Pt-Pd/C-TiO_2 exhibited comparable electrocatalytic activity for CO_2 reduction, and consequently a further distinction is not made between the two materials in the data trends presented next.

Cyclic voltammetry (data not shown) of 0.2 M NaF solutions (pH = 5.3) containing 50 mM pyridinium cation (PyH^+) revealed the onset of the $1e^-$ reduction of the cation to the neutral pyridinium radical at *ca.* −0.5 V on both Pt and Pd surfaces. Remarkably, an unmodified glassy carbon surface is completely inactive toward electroreduction of the pyridinium cation. Figure 11.8 compares hydrodynamic voltammograms (at 1200 rpm rotation speed) for a Pt/C-TiO_2

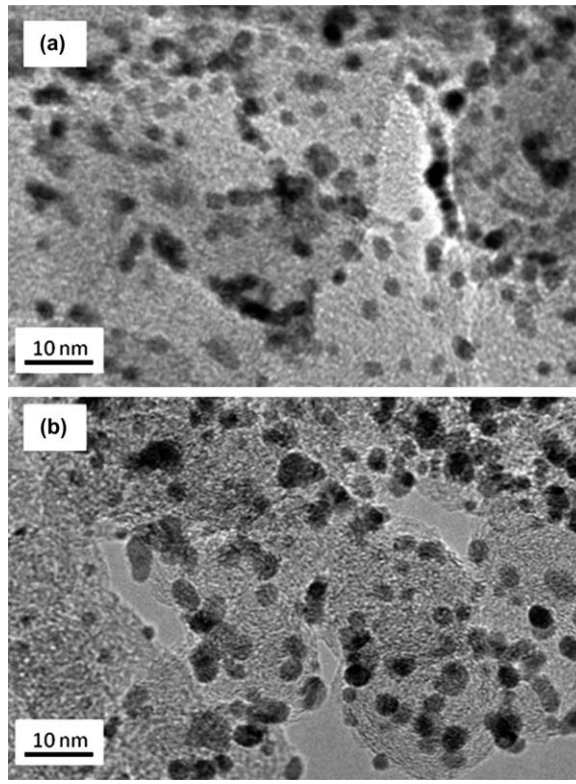

Figure 11.7 HR-TEM images of (a) Pt/C-TiO_2 and (b) Pd-Pt/C-TiO_2 nanocomposite surfaces.
Reproduced from *Electrochem and Solid-State Lett*., 2012, **15**, B5–B8 with copyright permission of ECS, The Electrochemical Society.

RDE and a comparably-sized Pt RDE in 10 mM pyridine-loaded NaF supporting electrolyte saturated with either N_2 or CO_2. The Pt/C-TiO_2 nanocomposite contained 10 μg Pt dispersed on 0.196 cm^2 of the glassy carbon rotating disk electrode (RDE) surface, whereas the comparably-sized Pt RDE translated to a Pt content of *ca.* 3–4 mg, depending on the metal thickness.

As seen in Figure 11.8, addition of CO_2 led to marked enhancement of the cathodic current for both cathode materials, attesting to the catalytic role played by both Pt and the pyridine co-catalyst toward CO_2 reduction. In particular, note the *ca.* 30% enhancement in cathodic current flow for the Pt/C-TiO_2 nanocomposite relative to the massive Pt electrode case. This enhancement occurred in spite of the fact that the loading of Pt in the Pt/C-TiO_2 electrode is approximately a *million-fold* less than that corresponding to a Pt RDE. Thus the mass activity of Pt/C-TiO_2 as expressed by the current density normalized by the mass of platinum at -0.55 V were 46.4 and 76.6 $mA.mg^{-1}$ in N_2 and CO_2 respectively, whereas for the Pt disk (assuming $\sim$1 g of metal content) the corresponding values were 1.44×10^{-4} and 2.51×10^{-4} $mA.mg^{-1}$, respectively.

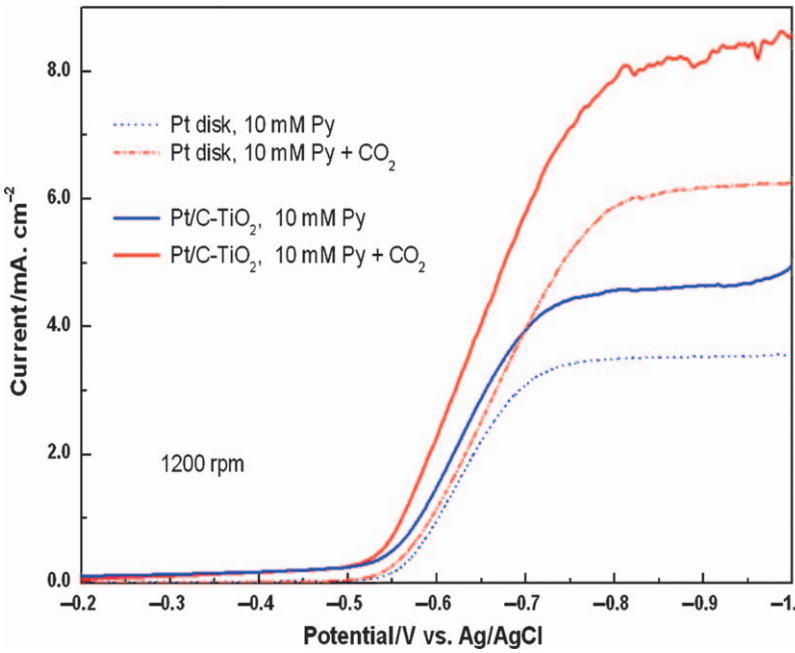

Figure 11.8 Comparison of hydrodynamic voltammograms for a Pt/C-TiO_2 nanocomposite RDE with a Pt RDE in PyH^+-loaded NaF solutions saturated with N_2 and CO_2 respectively.
Reproduced from *Electrochem and Solid-State Lett*., 2012, **15**, B5–B8 with copyright permission of ECS, The Electrochemical Society.

Significantly, close examination of the hydrodynamic voltammogram in the plateau region in Figure 11.8 for the Pt/C-TiO_2 case in the presence of CO_2, showed noise that is consistent with the visual observation of gas bubbles (presumably CO and/or H_2) on the electrode surface. Comparable data trends were seen in the Pt-Pd/C-TiO_2 *bimetallic* case, although Pt outperformed Pd alone in this regard (data not shown). The hydrodynamic voltammetry trends shown in Figure 11.8 were elaborated further for Pt/C-TiO_2 using variable rotation rates, and the corresponding data are presented in Figure 11.9. Once again, the cathodic current enhancement was seen at all rotation speeds, and noise in the plateau region is unmistakable when CO_2 is present in the electrolyte (compare Figure 11.9 a and b). The increase in current flow observed at potentials more negative than -0.9 V in Figure 11.8 and is associated with proton reduction (and hydrogen evolution).

Figure 11.10 shows Levich plots[51] (constructed from the hydrodynamic voltammetry data in Figure 11.9) of the limiting current density, j_L *vs.* the square root of the electrode rotation speed for the Pt/C-TiO_2 nanocomposite cathode in N_2 and CO_2 saturated solutions.

$$j_L = 0.62\,\mathrm{n\,F D^{2/3} \nu^{-1/6} C\,\omega^{1/2}} \qquad (11.7)$$

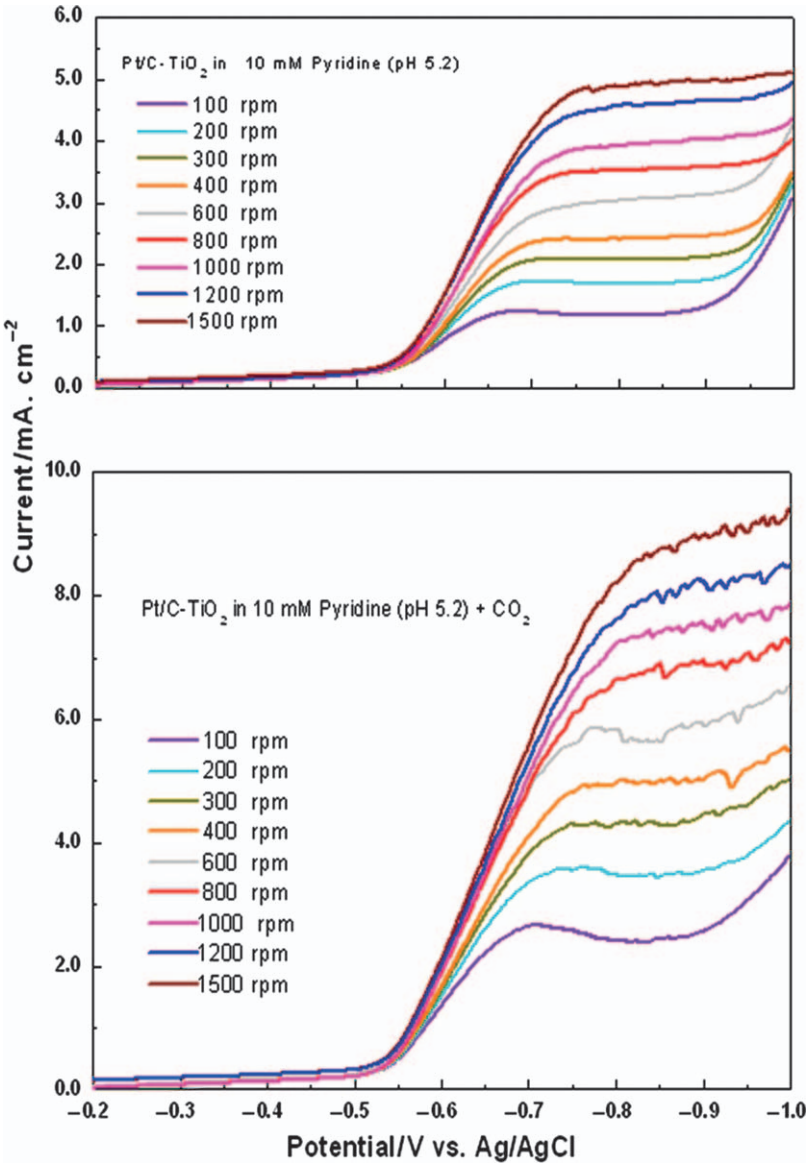

Figure 11.9 Hydrodynamic voltammetry data for a Pt/C-TiO_2 RDE in 10 mM PyH^+ -loaded aqueous solutions (NaF, pH 5.3) saturated with N_2 (top) and CO_2 (bottom), respectively.
Reproduced from *Electrochem and Solid -State Lett*, 2012, **15**, B5–B8 with copyright permission of ECS, The Electrochemical Society.

In Equation (11.7), n is the number of electrons transferred, F is the Faraday constant, D is the diffusion coefficient of the electroactive species (PyH^+), ν is the kinematic viscosity of the electrolyte ($\sim 0.01\,cm^2\ s^{-1}$),[51] C is the PyH^+

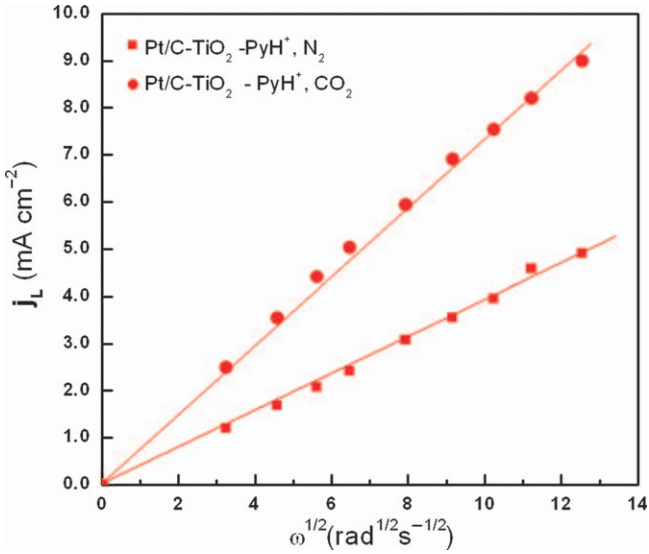

Figure 11.10 Comparison of Levich plots for the electroreduction of PyH^+ in N_2 and CO_2 saturated solutions using a Pt/C-TiO_2 RDE. Slopes and correlation coefficients from least-squares fits are 0.401 $mAcm^{-2}\,s^{1/2}$ and 0.9986 and 0.718 $mAcm^{-2}\,s^{1/2}$ and 0.9987 for the N_2- and CO_2 saturated solutions respectively. Data for the Levich plots are taken from Figure 11.9. Reproduced from *Electrochem and Solid-State Lett*., 2012, **15**, B5–B8. with copyright permission of ECS, The Electrochemical Society.

concentration (mol cm^{-3}) at the respective solution pH and ω is the electrode rotation rate in radians s^{-1}. The values used for D and C were 7.6×10^{-6} $cm^2\,s^{-1}$ and 0.8×10^{-5} mol cm^{-3}, respectively.[52]

As seen in Equation (11.7), a plot of j_L *vs.* $\omega^{\frac{1}{2}}$ (Levich plot) should be linear for diffusion-controlled electrochemical processes. Both sets of data in Figure 11.10 show good linearity; the slopes of the two Levich plots afford values for the electron stoichiometry (n) which are very close to 1.0 and 1.8 in N_2 and CO_2 saturated solutions respectively. Clearly, the pyridinium-catalyzed CO_2 reduction is sustained by the initial diffusion-controlled one-electron reduction of PyH^+ to $PyH^\bullet$ radical on Pt/C-TiO_2. Importantly, the nanocomposite electrocatalyst layer was thin enough (0.05–0.08 μm range) to not contribute to film diffusion-limited behavior.[49,53] Further implications of the data in Figure 11.10 require follow-up work.

The good stability of the nanocomposite electrodes were confirmed by recording the electrode potential during a 50-h galvanostatic electrolysis run. Only a minor and gradual potential drift (from −0.50 V to −0.58 V) was observed, attesting to the good stability of the nanocomposite material. It is worth underlining that as these galvanostatic electrolyses were performed at low current density, the electrode potential remained near the bottom of the hydrodynamic current–potential regime (see Figure 11.8 and Figure 11.9), thus involving mainly the reduction of pyridine without much interference from H_2

formation at the nanocomposite surface. As the solution was intentionally not buffered to avoid interference in alcohol detection, this small potential drift probably reflects a progressive increase of pH with time due to the consumption of protons associated with product generation.

Gas chromatography (GC) analyses of the electrolysis solution revealed the formation of both methanol and isopropanol as solution products at the Pt/C-TiO_2 nanocomposite cathode Figure 11.11(a). As shown in Figure 11.11 a, at

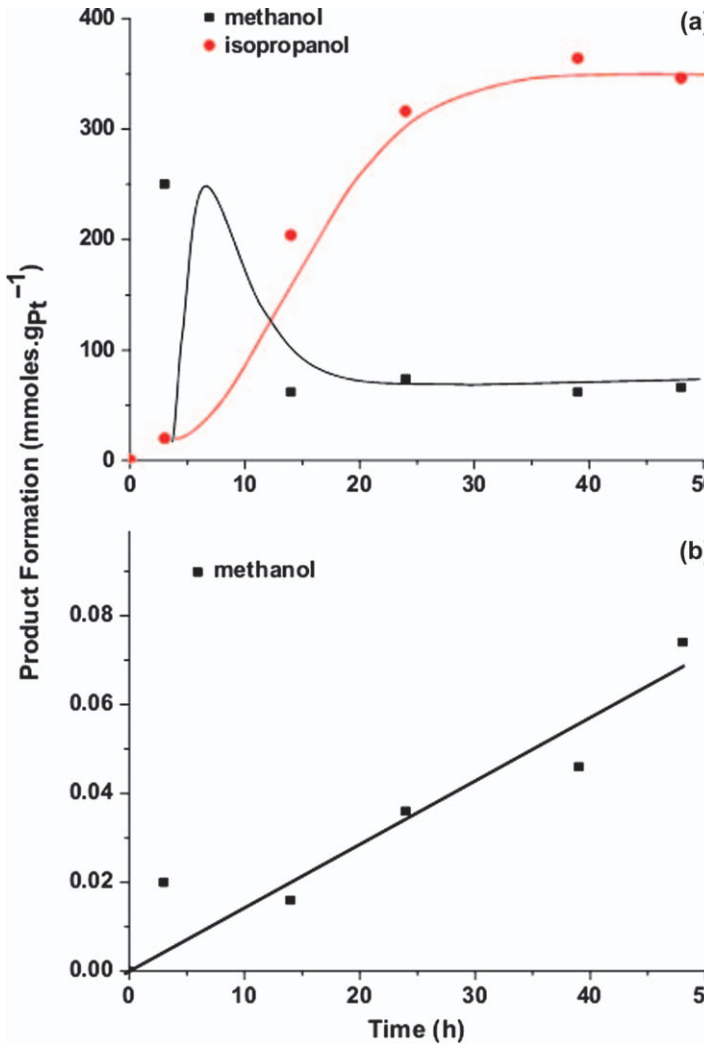

Figure 11.11 GC analyses as a function of time for constant-current electrolysis of CO_2-saturated solutions using: (a) Pt/C-TiO_2 and (b) Pt foil cathodes. Electrolysis conditions specified in the text.
Reproduced from *Electrochem and Solid-State Lett*., 2012, **15**, B5–B8 with copyright permission of ECS, The Electrochemical Society.

short reaction times ($t < 1$ h), methanol is the major product with lesser amounts of isopropanol. Subsequently, the amount of methanol drops precipitously, whereas the isopropanol content increases regularly. This drop in methanol content could arise from volatilization and entrainment of methanol in the CO_2 stream (due to constant CO_2 bubbling). This would be less of an issue with isopropanol due to its higher vapor pressure, and as seen in Figure 11.11a, the concentration of isopropanol increases regularly up to 40 h, after which production is flat throughout the electrolysis.

Only methanol was seen as the CO_2 electroreduction product in the Pt foil case (Figure 11.11(b)). Importantly, no CO was seen in the final reduction products in either case in Figure 11.11a and b. This is especially significant in that metals such as Pt or Pd are known to produce CO selectively on electroreduction of CO_2.[54] Clearly, the nanocomposite matrix facilitates deeper reduction (to alcohols) beyond the $2e^-$ CO stage. The mechanistic factors underlying this trend will be probed further in follow-on work that is planned in the Rajeshwar laboratory. Specifically, one intriguing aspect of these data is that *multi-carbon* products such as isopropanol are generated in the Pt/C-TiO_2 nanocomposite case, whereas Pt generates only methanol. Clearly the intermediate products from the initial reduction remain in close proximity to the interface in the former case so that subsequent product coupling can occur.

Finally, we note that the production of alcohol per unit mass of Pt for the nanocomposite matrix case (Figure 11.11(a)) is *three orders of magnitude* larger than the Pt foil case (Figure 11.11(b)). This represents substantial reduction in Pt usage and is an important practical advance toward improving the economics of electrochemical reduction of CO_2 to liquid fuels. Thus, the data discussed above show for the first time that nanocomposite cathode matrices derived from either Pt/C-TiO_2 or Pt-Pd/C-TiO_2 are effective electrocatalysts for aqueous CO_2 reduction in the presence of a solution co-catalyst such as the pyridinium cation. It is worth noting in this regard that matrices such as carbon black have good adsorption affinity for CO_2[55] pointing to synergistic factors such as the site-proximity effect[56] being operative for nanocomposite matrices such as the ones developed in this particular proof-of-concept study.

11.6 Transition Metal Complexes for Photocatalytic CO_2 Reduction

11.6.1 Catalysts for Reduction of CO_2 to CO or $HCOO^-$

Compared to the number of electrocatalysts for CO_2 reduction, photochemical catalysts are far more limited and are largely limited to Re and Ru complexes. Table 11.2, to the best of our knowledge, contains a collection of all reported molecular photocatalytic systems for CO_2 reduction. Of the 42 systems reported, only 5 systems do not involve Re or Ru. Three utilize the organic chromophores phenazine and para-terphenyls and two utilize Fe- and Co-based porphyrins. In most cases, the chromophore is coupled with a CO_2-reducing co-catalyst which is a known electrocatalyst for CO_2 reduction. CO,

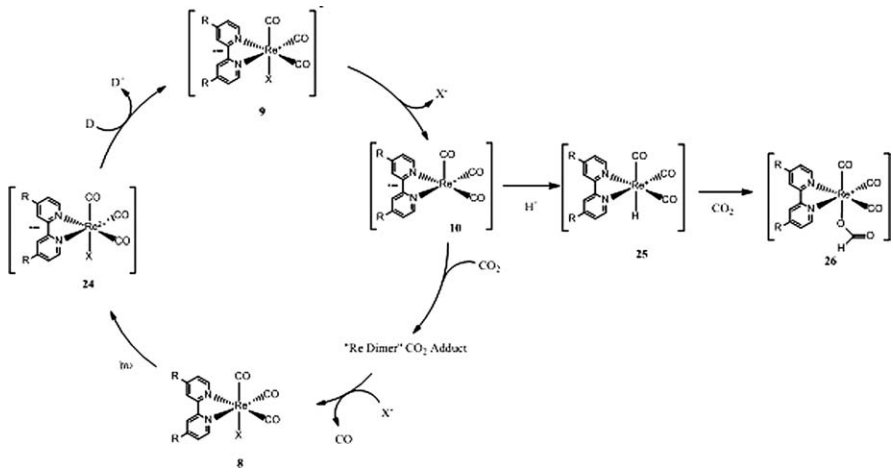

Figure 11.12 Photocatalytic cycle of *fac*-Re(bpy)$(CO)_3$X with the formation of the formate adduct.

formate, and H_2 are the only reported products for these systems, with the sole exception of entry #15, indicating that deeper reduction has remained an elusive goal. In most of these systems, CO formation is proposed to occur *via* the disproportionation of the $CO_2^{\bullet -}$ radical anion[34] or a two-electron reduction to produce CO.[57–61]

One of the better studied photocatalysts is *fac*-$[Re(bpy)(CO)_3X]^+$ which is also one of the few systems in which the chromophore is also the CO_2 reducing catalyst. Hori[62] and Lehn[29,63,64] have proposed the mechanism shown in Figure 11.12 for the production of CO. After reductive quenching of the photoexcited state (**24**), dissociation of the halide forms the coordinatively unsaturated species **10** which then can react with CO_2. While the exact structure of the CO_2 complex is not fully known, one proposed structure is the μ_2-η^2-CO_2 bridged binuclear Re adduct.[29,62–64] In any case, the CO_2 adduct is unstable and decomposes to yield CO and **8**. Ishitani proposes a similar mechanism except that **10** adds CO_2 and instead of dimerization as a method to provide a second reducing equivalent, the CO_2 adduct is reduced a second time by an outer-sphere mechanism to yield CO and complex **8**.[65] At present, both mechanisms have reasonable data to support their claims.[27] Among a related rhenium photocatalyst family, *fac*-$[Re(bpy)(CO)_3P(OEt)_3]^+$ has been demonstrated to be most efficient.[60,66–68] The one electron reduced species is almost quantitatively produced and is unusually stable in solution because of the strong electron-withdrawing property of the $P(OEt)_3$ ligand.[60,66–68]

A competing reaction in this system is the reaction of species **10** with a proton to give the metallo-hydride (species **25**).[29] This species can react with a proton to give hydrogen gas,[29] or it can insert CO_2 to give the metallo-formate complex (species **26**), which kills the catalyst as the formate is not released.[29,64] Hori and coworkers noted that it was possible to prevent this deactivation

pathways, *i.e.* inhibit hydride formation, by increasing the CO_2 partial pressure.[62] Catalyst turnover exhibited a 5-fold improvement at 54 atm over a 1 atm system.

One issue with the Re photocatalysts is the limited range of absorption in the visible region, which is typically limited to wavelengths below 440 nm. Multinuclear metal supramolecular complexes were developed for CO_2 reduction photocatalysts for this reason. These complexes were composed of a photosensitizer part, a ruthenium(II) bpy-type complex, and a catalyst part based on the of rhenium(I) tricarbonyl complexes. A number of bi-, tri-, and tetranuclear complexes linked by several types of bridging ligands have been investigated in the literature (Figure 11.13).[60,69–74] The bridging ligands strongly influence photocatalytic ability, including selectivity of CO over H_2, high quantum yields and large turn over numbers, of the complexes. In all of these complexes, the ^{3}MLCT excited state of the ruthenium moiety was reductively quenched by a sacrificial reducing agent and the one electron reduced Re complex was formed through intramolecular electron transfer from the reduced Ru chromophore.[60] Ishitani *et al*. have shown that the catalytic activity of these mixed Re/Ru assemblies improves upon increasing the Re/Ru ratio, presumably due to the ready availability of Re sites (which catalyzes the slow step) to pick up electrons from the photoreduced Ru site (the fast step).[69,71,72]

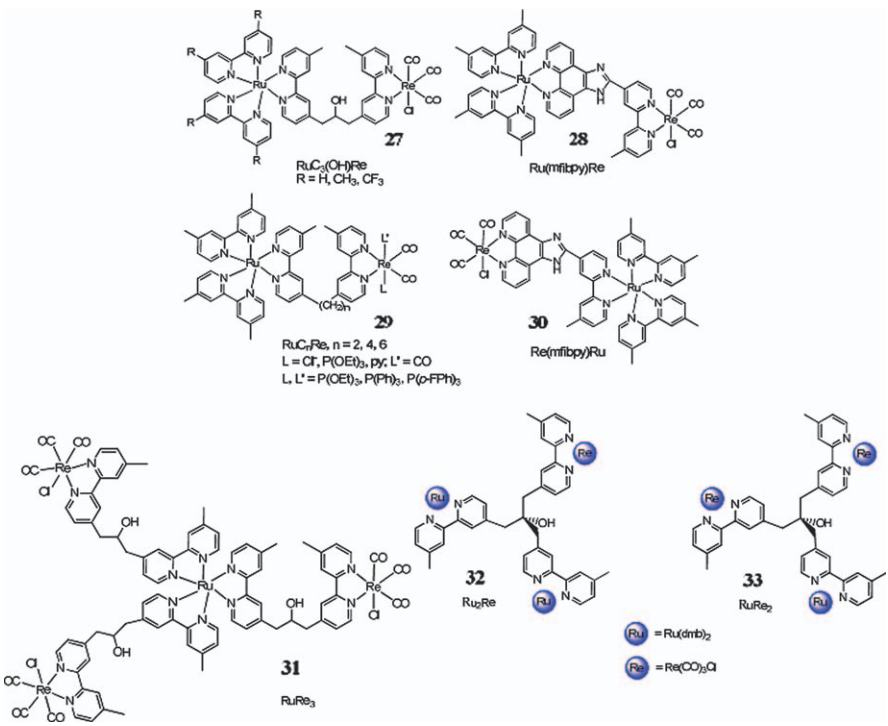

Figure 11.13 Chemical structures of multinuclear rhenium complexes.

Table 11.3 TON_{CO} of different numbers of active sites and their comparison with appropriate monometallic model complexes containing different ratios of $[Ru(dmb)_3]^{2+}$ and $[(dmb)Re(CO)_3Cl]$. TON is calculated after 16 h of irradiation based on Ru(II) moieties with the complex concentration of 0.05 M.

Complexes	*Ru + Re (1:1)*	*Ru-Re*	*Ru + Re (1:2)*	*Ru-Re$_2$*	*Ru + Re (1:3)*	*Ru-Re$_3$*	*Ru + Re (2:1)*	*Ru$_2$-Re*
TON_{CO}	100	160	89	190	60	240	55	110

Moreover, a comparison of each multinuclear system to their corresponding system composed of the individual components shows that the intramolecular system is superior as shown in Table 11.3.[69–71] The electronic structure of the bridging ligands is important and systems in which there is strong electronic communication between metal sites perform less well than those with weak electronic coupling.[69,70] Thus, the more conjugated bridging is not better for supramolecular architecture for photochemical CO_2 reduction.[73] In order to direct the electron towards the Re center in the Ru/Re assemblies, it is important to adjust the π^* orbital energy on peripheral bpy ligands of the Ru chromophores, such that they do not become electron traps.[69] Ideally, the acceptor orbital of the bpy-like portion of the bridging ligand should be equal or lower in energy than that of the peripheral ligands to help direct the electron to the Re site.[60,69]

Cyclam-based macrocyclic ligands with either cobalt or nickel ions are one of the most commonly used co-catalysts for the photochemical reduction of CO_2 in the presence of $Ru(bpy)_3^{2+}$.[75–83] As seen in Figure 11.14,[78] the production of CO is shown to proceed through the reduction of the macrocycle by the singly reduced Ru species, $Ru(bpy)_3^{+}$, followed by formation of metal hydride intermediate (species **36**). The next step is insertion of CO_2 into the metal hydride bond to form the metallo-formate (**37**). This species then decomposes to form CO and water. This species can rearrange to for the oxygen-bound formate species **38** which can be lost as formate by simple protonation.[75,77,78,82,84] In both cases, the catalyst is regenerated by a reducing agent. A competing pathway in this system is the reaction between the metal hydride and another proton to form H_2. The use of a different photosensitizer yields an additional product with these catalysts. When *p*-terphenyl[81,83] or phenazine[82] is used in place of $Ru(bpy)_3^{2+}$ the formation of formate is also observed in addition to CO and H_2.

Another class of macrocycle complexes that are used in the reduction of CO_2 are porphyrin-based complexes using iron and cobalt. The photochemical reduction of CO_2 with iron porphyrins, follows a similar catalytic process as the electrochemical reduction, shown in Figure 11.15, with the key difference being the method in which the active species, $[Fe(0)TPP]^{2-}$, is formed.[85] In the photochemical method, the active species is formed through a three-step process which involves four photons and two porphyrin rings. The first step (Equation (11.8)) is photoreduction of the iron(III) porphyrin to iron(II)

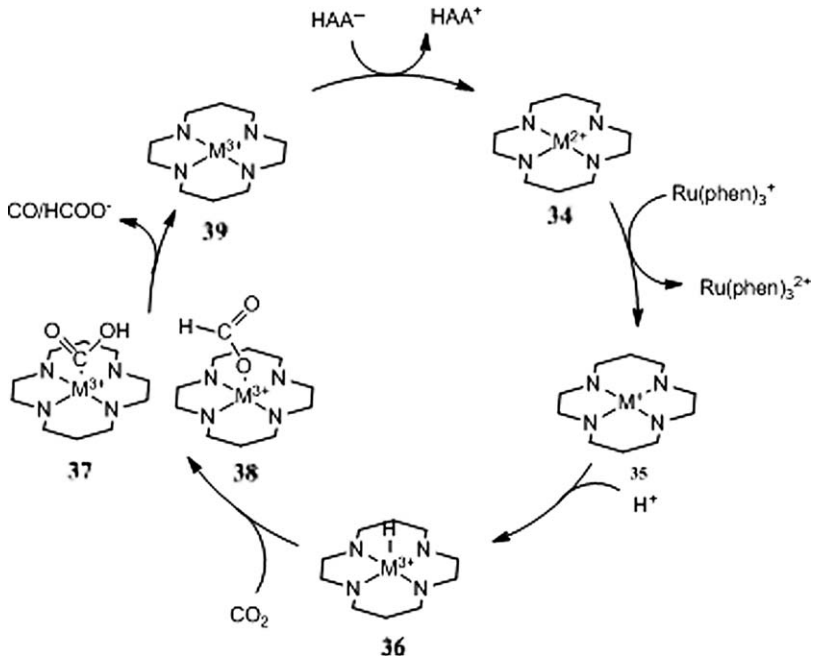

Figure 11.14 Acid assisted CO_2 electroreduction by metal cyclam where M is cobalt or nickel.

porphyrin in the presence of a reducing agent, TEA, which is coordinated to the axial site of the complex.

The second step is further illumination of the iron(II) species to result in iron(I) species with a mechanism similar to first step (Equation (11.9)). This process is far less efficient than the previous one and is affected by the concentration of TEA.

$$\text{TEA-Fe(III)TPP} \xrightarrow{\text{hv}} \text{Fe(II)TPP} + \text{TEA}^{\bullet+} \tag{11.8}$$

$$\text{TEA-Fe(II)TPP} \rightarrow \text{Fe(I)}\overset{\text{hv}}{\text{TPP}}^{-} + \text{TEA}^{\bullet+} \tag{11.9}$$

The last step to make the active species of this complex is a disproportionation reaction of two iron(I) species in solution to give one iron(0) species and one iron(II) species (Eqn. 11.10). CoTPP, was demonstrated to perform similarly to FeTPP with $Co(0)TPP^{2-}$ as the active catalytic species.[84]

$$2\text{Fe(I)TPP}^{-} \rightarrow \text{Fe(0)TPP}^{2-} + \text{Fe(TPP)} \tag{11.10}$$

11.6.2 Deeper Reduction Using a Hybrid System

As mentioned previously, molecule-based photochemical systems capable of photoreducing CO_2 beyond formic acid or CO are hard to come by. In recent

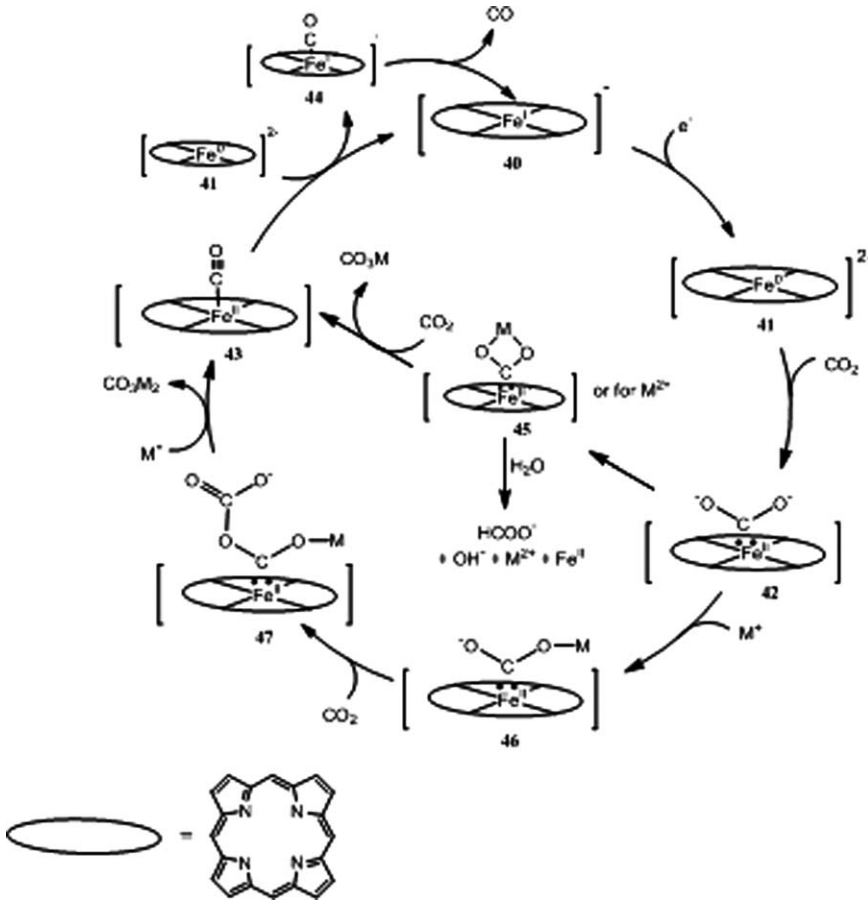

Figure 11.15 Metal ion-assisted CO_2 reduction where the metal ion is Ca^{2+}, Mg^{2+}, Na^+, Li^+, with Mg^{2+} working the best.

work, we examined the use of pyridine and the $[Ru(phen)_3]^{2+}$ chromophore for reduction of CO_2 to methanol, basing the deeper reduction on the prior work of Bocarsly *et al.* (see section 11.4.1).[86] As shown in Figure 11.16, methanol was produced in a system composed of $[Ru(phen)_3]^{2+}$, pyridine, ascorbic acid, and CO_2 in water (pH 5.0) irradiated at 470 nm over a period of 6 h.[86] The proposed mechanism of reduction is indicated in Figure 11.17; the entire system is seen to be simply a combination of the CO_2-reducing ability of pyridine and the reducing power of $[Ru(phen)_3]^+$ formed upon reductive quenching of the ^{3}MLCT state in the complex. Interestingly, this is the first report of pyridine functioning to produce methanol in a purely molecular system. In the electrocatalytic systems, it has been reported that the nature of the working electrode is integral to the observed catalytic activity. For example, methanol production is only

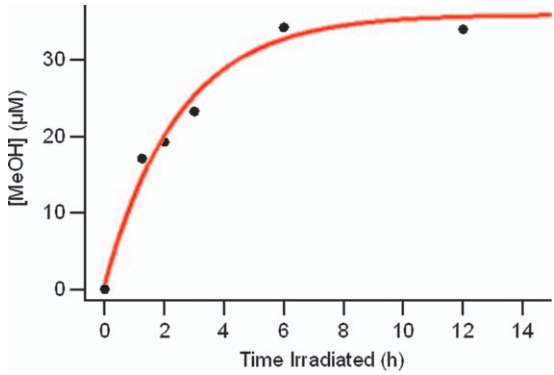

Figure 11.16 Temporal evolution of methanol from reduction of CO_2 with time for irradiation with 470 nm light.

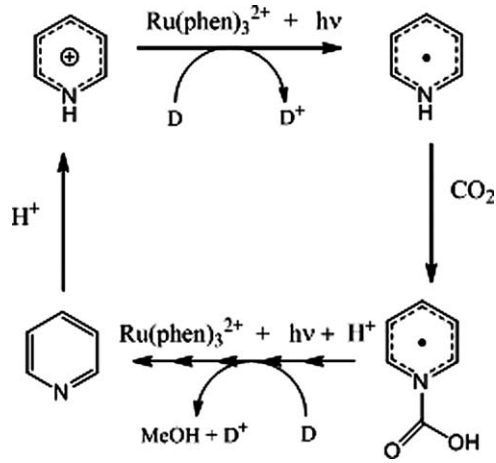

Figure 11.17 Proposed mechanism of the reduction of CO_2 by pyridine in the presence of $[Ru(phen)_3]^{2+}$ in water.

observed with Pt working electrodes, and theoretical studies have suggested that the Pt surface is required for methanol production.[86] At present, the activity of the $[Ru(phen)_3]^{2+}$/pyridine system is modest, with 0.15 methanol molecules produced per Ru chromophore over a 6 h period, which – when adjusted for the number of electrons involved – corresponds to 0.9 TON.[86] The loss of activity after 6 h is attributed to decomposition of the $[Ru(phen)_3]^{2+}$ chromophore, which is known to occur *via* ligand labilization in the excited state, a problem than can exacerbated by the presence of pyridine in the system. Reports of deeper reductions of CO_2 to methane are quite rare in the literature, although the process has been observed for the $[Ru(bpy)_3]^{2+}$ chromophore and colloidal metals.[87,88]

11.7 Photocatalytic CO_2 Reduction using Semiconductor Nanoparticles

11.7.1 Syngas as Precursor in Fisher-Tropsch Process for Production of Synthetic Fuels

Syngas (or ''synthesis gas'') is the name given to a gas mixture that contains varying amounts of CO and H_2. Common examples of producing syngas include the steam reforming of methane or liquid hydrocarbons and the gasification of coal or biomass. Thermally mild (*i.e.* low temperature) alternatives for producing this transportable chemical fuel mixture would obviously be significant from an energy perspective. Value is added even further if the production process can be driven *via* a renewable solar energy source from a source greenhouse gas material such as CO_2.

11.7.2 Photogeneration of Syngas Using $AgBiW_2O_8$ Semiconductor Nanoparticles

Figure 11.1 depicts the band-edges for $AgBiW_2O_8$ superimposed on the relevant redox levels for CO_2 reduction. Unlike for semiconductors such as WO_3 and $BiVO_4$ that are otherwise excellent photocatalysts for oxidative processes (*e.g.* water photooxidation), the conduction band-edge of $AgBiW_2O_8$lies far enough negative to sustain CO_2 reduction.

Double tungstates of mono- and trivalent metals with composition: $AB(WO_4)_2$ are known to have structural polymorphism.[89] Here, A is a monovalent alkali metal (or Ag, Tl) and B represents a tri-valent element such as Bi, In, Sc, Ga, Al, Fe, or Cr. To date, very little is known on the exact crystal structure of $AgBiW_2O_8$. Our density functional theory calculations[90] indicate that the wolframite structural modification should be the most stable, while the scheelite and fergusonite structures are 0.69 eV and 0.28 eV higher in energy, respectively. Further details are given in reference 90. Synthesis, structural, surface, and optical characterizations of this oxide semiconductor are also given elsewhere.[90,91] We focus here on the use of nanosized particles of Pt-modified $AgBiW_2O_8$ for mild syngas photogeneration.

Formic acid was used as a precursor for CO_2 in these proof-of-concept experiments. The UV-photogenerated holes in $AgBiW_2O_8$ were then used to generate CO_2 in situ at the oxide semiconductor-solution interface. It is worth noting here that the direct electrochemical reduction of CO_2 in aqueous media is hampered both by the low partial pressure of CO_2 in the atmosphere (3.9×10^{-4} atm) and by its low solubility in water (1.5 g/L at 298 K).[92] On the other hand, formate species have high solubility in water (945 g/L at 298 K).[93] Further, they have high proclivity for being adsorbed on oxide semiconductor surfaces[94] and are easily oxidized by the photogenerated holes in the oxide. Figure 11.18 presents the data.[90,91] The GC results clearly show the formation of CO and H_2 *via* photocatalytic reactions. Control experiments conducted without

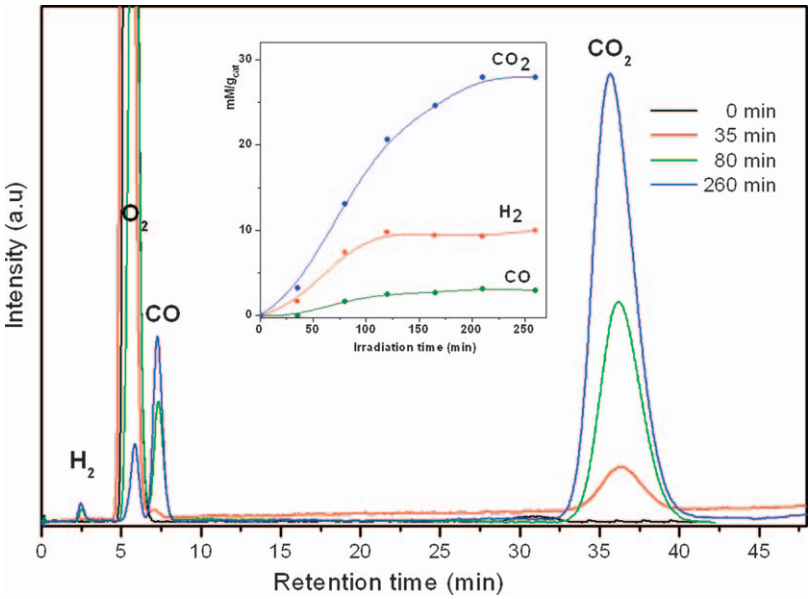

Figure 11.18 GC data for the simultaneous evolution of CO and H_2 from a platinized $AgBiW_2O_8$ suspension.
Reproduced with copyright permission from *J. Nano Research,* 2012, **17**, 185–191, Trans Tech Publications, Switzerland.

the oxide semiconductor did not yield any of the products shown in Figure 11.18, indicating that direct photolysis of the organic acid was not a factor here.

One surprising aspect of these experiments was that product generation could be sustained for periods up to at least several minutes without a noticeable fall-off in the rate. This indicates that CO-poisoning of the Pt surface was not a factor, at least in the initial stages of the photocatalytic process. The site specificity of product evolution, namely HER on the Pt sites and CO_2 photoreduction on the unmodified oxide surface, is an interesting aspect that deserves further study. The results in Figure 11.18 are also non-optimized in terms of product evolution efficiency and quantum yield. Practical application of this syngas photogeneration approach will necessitate modification of the oxide semiconductor so that wavelengths in the visible part of the solar spectrum (rather than the UV portion in Figure 11.18) can be accessed.

11.7.3 Photoreduction of CO_2 using Cu_2O as Semiconductor and Pyridine as Solution Co-Catalyst

Copper (I) oxide, Cu_2O, is an attractive p-type semiconductor with a band gap energy of $\sim$2.0 eV, a conduction band-edge lying far enough negative to sustain CO_2 reduction, and a high absorption coefficient over the visible wavelength range in the solar spectrum. One limitation of using Cu_2O photoelectrodes is their poor stability in aqueous electrolytes because the redox potentials for

Cu_2O/Cu^0 and CuO/Cu_2O lie within the band gap of thee semiconductor. However, the performance of these photoelectrodes can be enhanced by metal and/or semiconductor coatings[95, 96] as well as by solution electron shuttles such as methyl viologen.[96] We reported the stabilization of electrodeposited Cu_2O photoelectrodes by a Ni surface protection layer and also by the use of an electron shuttle in solution.[96] High photoactivity of electrodeposited Cu_2O was obtained under a surface protection consisting of nanolayers of Al-doped ZnO and TiO_2 to avoid photocathodic decomposition.[95] These films were also activated with Pt nanoparticles to enhance solar hydrogen generation.[95] Photocurrents for electrodeposited $Cu_2O(111)$ were optimized separately for solar H_2 generation without using any surface treatment.[97]

Cathodic electrodeposition of copper oxide from a copper sulfate bath containing lactic acid is a versatile and low-cost technique. The bath pH is known to determine the grain orientation and crystallite shape of the resulting film.[97–100] Thus, films electrodeposited from an alkaline bath of pH ~ 9 are highly oriented along the (100) plane, while a preferential (111) orientation occurs in films grown at more alkaline pHs (pH ~ 12).[98] Interestingly, as the bath pH is varied from 7.5 to 12, a third preferred orientation, (110), can be identified in a narrow pH range of 9.4 to 9.9.[101] The preferred grain orientation and crystallite shape were also found to depend on the applied potential (in the potentiostatic growth mode),[102] while layered Cu_2O/Cu nanostructures were formed by galvanostatic electrodeposition.[103]

Although there are quite a few studies on the use of Cu_2O photocathodes for HER,[96,97,104–106] to the best of our knowledge there are no reports of their use for CO_2 photoreduction. An intriguing aspect for study hinges in the capability of preferentially-oriented electrodeposited films for CO_2 photoreduction. Among the (100), (110) and (111) crystal faces of Cu_2O, the (111) orientation is the best one for photoreduction reactions,[107] and therefore the data presented below correspond to electrodeposited $Cu_2O(111)$ films. Besides, the observation of high cathodic photocurrents ($\sim$ 6–8 mA/cm^2) for HER on $Cu_2O(111)$ films electrodeposited from a copper lactate solution (pH 12)[95–97] is very encouraging because it demonstrated that the highest cathodic photocurrent were associated with electrodeposited Cu(111) films.[97]

The use of a p-type photoelectrode for CO_2 reduction was reported in the late eighties for the case of CdTe and GaP electrodes in aqueous solutions in the presence of tetraalkylammonium salts.[108] However, much more recently, pyridine was incorporated into the electrolyte as a co-catalyst for the reduction of CO_2 at illuminated p-type electrodes (GaP and FeS_2).[109,110]

Our data below correspond to electrodeposited $Cu_2O(111)$ films grown on gold-coated quartz crystal working electrodes polarized at –0.4 V in 0.2 M $CuSO_4$ + 3 M lactic acid + 0.5 M K_2HPO_4, pH 12 at 25 C to reach a total charge of 180 mC/cm^2 which corresponds to 0.25 μm film thickness. The associated total mass of the film was 140 μg/cm^2 as measured during its growth by electrochemical quartz crystal microgravimetry (EQCM).

To analyze the stability of electrodeposited $Cu_2O(111)$ electrodes, cathodic photocurrent density and mass change (Δm) were recorded as a function of

potential under chopped simulated AM 1.5 solar illumination in a solution just containing the supporting electrolyte (Figure 11.19).[111] Prior to defining the optimal film thickness, careful analyses were performed (data not shown) to verify compliance of the EQCM set-up with the Sauerbrey equation.[111–113]

Figure 11.19 compares the effect of solar light intensity on the photocurrent and Δm values for the photoelectroreduction of water to hydrogen. The data in Figure 11.19 (top) are for illumination from a 1.5 AM solar simulator, and those in Figure 11.19 (bottom) are for the case when a 10% neutral density filter was placed in between the light source and the electrochemical cell. Clearly, although significantly higher photocurrents (up to $2\,mA\,cm^{-2}$) are reached under full illumination, there is a beneficial effect on the relative photocurrent and mass changes brought about by decreasing the light intensity. The total photocurrent is mainly associated with photoelectron transfer to water, photogenerating H_2 as represented in Equation (11.11):

$$H_2O + 2e^- \rightarrow H_2 + 2OH^- \tag{11.11}$$

Nonetheless, there are also measurable mass changes associated principally with the photocathodic decomposition of the oxide as indicated in Equation (11.12):

$$Cu_2O + 2e^- + H_2O \rightarrow 2Cu + 2OH^- \tag{11.12}$$

Reaction (11.12) has the net effect of decreasing the photoactivity of the electrode.

The above data show that electrodeposited $Cu_2O(111)$ films are more stable and reached higher photon to current conversion ratios than under the full output of simulated AM 1.5 illumination. This effect on performance seems to be rooted in the better capability of the photoelectrode/electrolyte interface to deal with a lower photon flux because: (i) there is less photoconversion of Cu_2O to Cu^0 (Equation (11.12)) as indicated by a lower mass loss and (ii) a more efficient photocurrent is associated with the transfer the photogenerated electrons to the electrolyte, *i.e.* conversion of water to H_2 (Equation (11.11)) when the light intensity is low. It is useful to recall here that the minority-carriers (photoexcited electrons) are collected only over a distance corresponding to the sum of the space charge layer thickness and the electron diffusion length. For electrodeposited $Cu_2O(111)$ electrodes, this distance is always less than 100 nm in the potential range under study,[97] while the photon absorption depth near the band gap is much larger and in the micrometer range (1–2 μm).

For CO_2 reduction on illuminated $Cu_2O(111)$, chopped (0.2 Hz) and continuous AM 1.5 simulated solar illumination were used (Figure 11.20). The pH of the electrolyte was adjusted to pH 5 to compare CO_2 reduction in the absence and in the presence of protonated pyridine (PyH^+, $pKa = 5.5$) as solution co-catalyst. Chopped illumination at a potential of −0.4 V (a rather low potential for Reaction 7 to be dominant) shows that the presence of PyH^+ enhances the cathodic photocurrent associated to CO_2 reduction only by *ca.* 15 % (compare Figure 11.20 a and b). While the photocurrent enhancement by PyH^+ is modest, the PyH^+ contribution by draining the photoelectrons to the solution

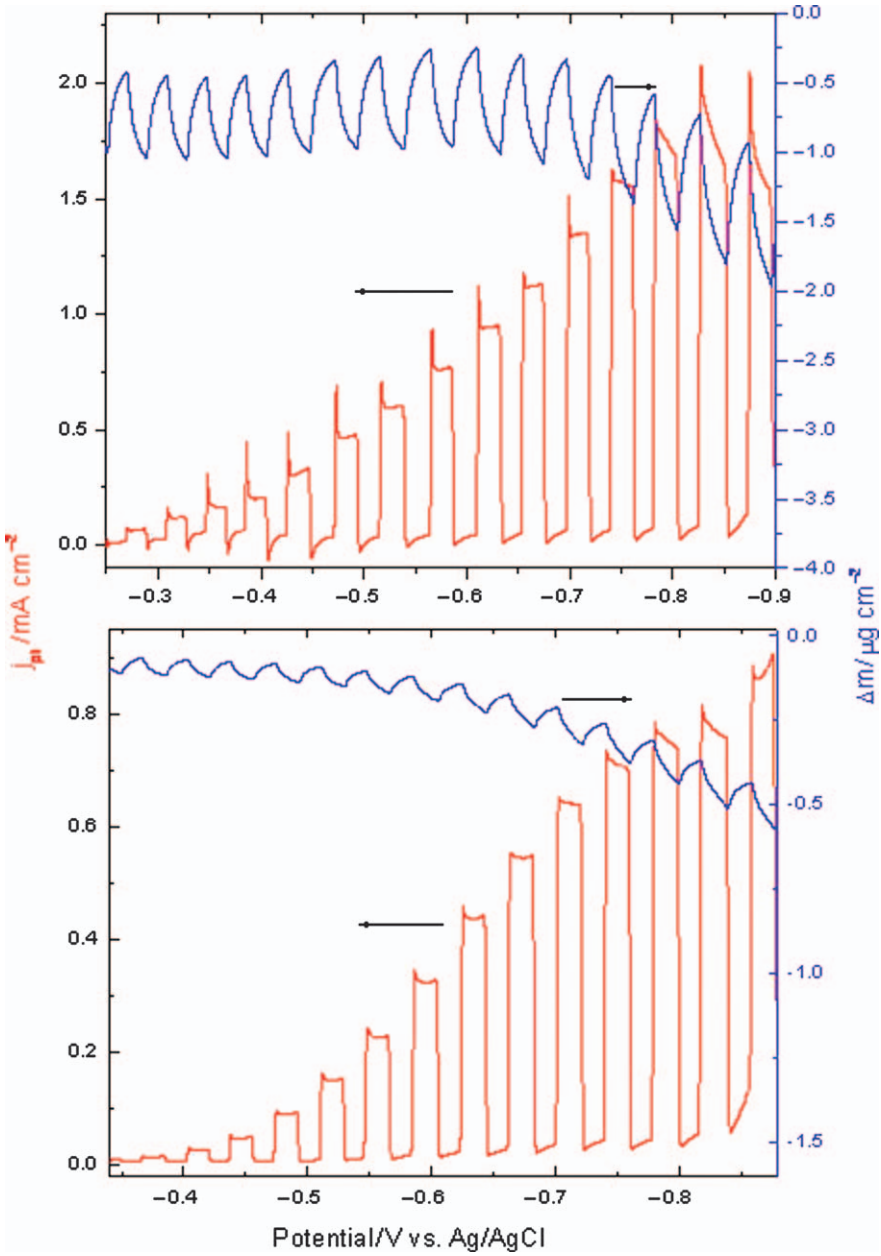

Figure 11.19 Effect of light intensity on the photocurrent/potential and Δm/potential profiles of $Cu_2O(111)$ films in N_2 saturated 0.1 M Na_3PO_4 under chopped simulated AM 1.5 illumination at full output (top) and at 10% intensity with a neutral filter (bottom).

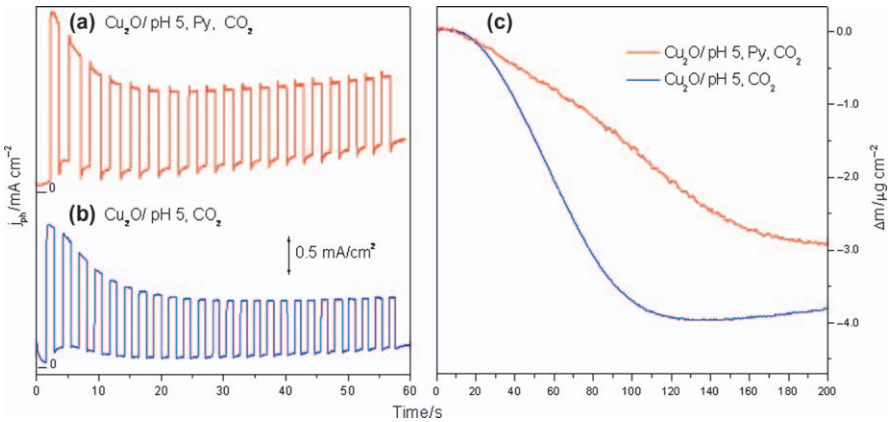

Figure 11.20 Photocurrent flow (under chopped 105 AM 1.5 illumination) at –0.4 V (*vs.* Ag/AgCl) for a $Cu_2O(111)$ film in pH 5, CO_2 saturated solution without (a, blue line) and with (b, red line) 10 mM pyridine. (Curves were shifted for better comparison and each one includes the zero current). Frame (c) contains a comparison of mass changes (as measured by EQCM) for the respective (a) and (b) scenarios except that continuous instead of chopped irradiation was used.

side, thus avoiding photocorrosion of the electrode, is quite clear as shown by the comparative mass changes under continous irradiation (Figure 11.20c). It can be seen that the mass decrease is faster in the absence of PyH^+, reaching a total mass loss of 4.0 μg/cm^2 after 120 s of irradiation, while in the presence of PyH^+ the mass loss was reduced to only 2.9 μg/cm^2 after 200 s.

Although these mass changes indicate the instability of the Cu_2O photoelectrodes, longer times of irradiation show only relatively insignificant mass changes, which in comparison to the total film mass (140 μg/cm^2) are only in the 2–3% range. Further, the presence of PyH^+ enhances the film inertness as indicated by the absence of mass increase associated with adsorption of solution species on the $Cu_2O(111)$ surface. Verification of these ideas is being carried out currently by analyzing the surface composition after performing CO_2 reduction as well as in the product detection from reactions such as those represented in Equation (11.12). Other Cu_2O film morphologies with different preferential orientations are also under scrutiny in our laboratory.

11.8 Concluding Remarks and Future Directions

Progress in the realm of molecular catalysts in the last 40 years toward the reduction of CO_2 has been substantial, but primarily limited to reduction to CO or formate. CO does have value in that it can be used in a Fischer–Tropsch reaction to produce higher carbon fuel products, but there is a general recognition that deeper reduction to more value-added products such as methanol is needed. Semiconductor-based photocatayst systems have also shown promise for both the above reduction pathways.

Although there are promising examples in the literatures, some obvious problems remain. The current technology does not meet the grand goal for industrial large-scale operation. The challenge to overcome is the overpotential for the electrochemical systems and short-lived one-electron reduced species for the photochemical systems. It is also critical to replace sacrificial reducing agents with more practical donors such as water, so as to close the loop in a practical fuel cycle. The use of sunlight to drive photoreduction is a sustainable method for the use of CO_2 as a C1 feedstock. Examples of incorporation of a chromophore with the real catalyst in either intermolecular or intramolecular photochemical systems have demonstrated the feasibility of CO_2 reduction. However, photoinduced electron transfer from the chromophore to the catalyst or from the semiconductor to the solution still account for much of the inefficiency in these systems. To address this issue will require sustained efforts by scientists in the rational design of molecule- or semiconductor-based assemblies to reduce these inefficiencies. It is the authors' hope that this book chapter will contribute to further progress and stimulate future generations of scientists to dvelop new electro-/photocatalyst design paradigms.

Acknowledgements

The authors would like to thank the National Science Foundation (CHE 0911720 to FMM, NT) and the Robert A. Welch Foundation (Y-1301 to FMM) for financial support.

References

1. M. E. Royer, *Comptes rendus hebdomadaires des séances de l'Académie des sciences*, 1870, **70**, 731.
2. A. d. s. (France), *Comptes rendus hebdomadaires des séances de l'Académie des sciences*, 1893, **116**, 1145.
3. H. H. Fenton, *J. Chem. Soc., Trans*, 1907, **91**, 687–693.
4. N. S. Spinner, J. A. Vega and W. E. Mustain, *Catal. Sci. Technol.*, 2012, **2**.
5. B. Kumar, M. Llorente, J. Froelich, T. Dang, A. Sathrum and C. P. Kubiak, *Annu. Rev. Phys. Chem.*, 2012, **63**, 541.
6. M. R. Hoffmann, J. A. Moss and M. M. Baum, *Dalton Trans.*, 2011, **40**, 5151.
7. E. B. Cole and A. B. Bocarsly, *Carbon Dioxide as Chemical Feedstock*, Wiley-VCH, Weinheim, 2011.
8. A. J. Morris, G. J. Meyer and E. Fujita, *Acc. Chem. Res.*, 2009, **42**, 1983.
9. E. E. Benson, C. P. Kubiak, A. J. Sathrum and J. M. Smieja, *Chem. Soc. Rev.*, 2009, **38**, 89–99.
10. T. Reda, C. M. Plugge, N. J. Abram and J. Hirst, *Proceedings of the National Academy of Sciences*, 2008, **105**, 10654.
11. Y. Hori, *Modern Aspects of Electrochemistry*, Springer, New York, 2008.
12. D. L. DuBois, in *Encyclopedia of Electrochemistry*, A. J. Bard and M. Stratmann, Wiley-VCH, Weinheim, 2007, vol. 7a , p. 202.

13. I. Taniguchi, *Mod. Aspects Electrochem.*, 1989, **20**, 327–400.
14. J. P. Collin and J. P. Sauvage, *Coord. Chem. Rev.*, 1989, **93**, 245–268.
15. M. D. Doherty, D. C. Grills, J. T. Muckerman, D. E. Polyansky and E. Fujita, *Coord. Chem. Rev.*, 2010, **254**, 2472–2482.
16. J. O. M. Bockris and J. C. Wass, *J. Electrochem. Soc.*, 1989, **136**, 2521.
17. K. Chandrasekharan and J. O. M. Bockris, *Surface Science*, 1987, **185**, 495.
18. K. Rajeshwar, in *Encyclopedia of Electrochemistry*, S. Licht, Wiley-VCH, Weinheim, 2001, pp. 3–53.
19. K. Rajeshwar, R. McConnell and S. Licht, *Solar Hydrogen Generation: Toward a renewable Energy Future*, Kluwer Academic, New York, 2008.
20. R. F. Service, *Science*, 2011, **334**, 925–927.
21. N. Furuya and K. Matsui, *J. Electroanal. Chem.*, 1989, **271**, 181–191.
22. G. Seshadri, C. Lin and A. B. Bocarsly, *J. Electroanal. Chem.*, 1994, **372**, 145–150.
23. A. Gennaro, A. A. Isse and E. Vianello, in *NATO ASI Series*, A. J. L. Pombeiro and J. A. McCleverty, Kluwer, The Netherlands, 1992, vol. 385 , pp. 311–316.
24. A. J. Morris, R. T. McGibbon and A. B. Bocarsly, *ChemSusChem*, 2011, **4**, 191–196.
25. E. Barton-Cole, P. S. Lakkaraju, D. M. Rampulla, A. J. Morris, E. Abelev and A. B. Bocarsly, *J. Am. Chem. Soc.*, 2010, **132**, 11539–11551.
26. J. Hawecker, J.-M. Lehn and R. Ziessel, *J. Chem. Soc., Chem. Commun.*, 1984, 328–330.
27. B. P. Sullivan, C. M. Bolinger, D. Conrad, W. J. Vining and T. J. Meyer, *J. Chem. Soc., Chem. Commun.*, 1985, 1414–1416.
28. J. M. Smieja and C. P. Kubiak, *Inorganic Chemistry*, 2010, **49**, 9283–9289.
29. J. Hawecker, J. M. Lehn and R. Ziessel, *Helv. Chim. Acta*, 1986, **69**, 1990–2012.
30. P. Christensen, A. Hamnett, A. V. G. Muir and J. A. Timney, *J. Chem. Soc., Dalton Trans.*, 1992, 1455–1463.
31. R. Ziessel, *Nato ASI Series, Series C*, 1987, **206**, 113–138.
32. M. A. Scibioh and B. Viswanathan, *Photo/electrochemistry & photobiology in environment, energy and fuel*, 2002, 1–46.
33. C. Amatore, L. Nadjo and J. M. Saveant, *Nouveau Journal de Chimie*, 1984, **8**, 565–566.
34. P. A. Christensen, A. Hamnett and A. V. G. Muir, *J. Electroanal. Chem. Interfacial Electrochem.*, 1988, **241**, 361–371.
35. H. Ishida, K. Fujiki, T. Ohba, K. Ohkubo, K. Tanaka, T. Terada and T. Tanaka, *J. Chem. Soc., Dalton Trans.*, 1990, 2155–2160.
36. H. Ishida, K. Tanaka, M. Morimoto and T. Tanaka, *Organometallics*, 1986, **5**, 724–730.
37. H. Ishida, K. Tanaka and T. Tanaka, *Chemistry Letters*, 1985, 405–406.
38. H. Ishida, H. Tanaka, K. Tanaka and T. Tanaka, *J. Chem. Soc., Chem. Commun.*, 1987, 131–132.
39. K. Tanaka, *Kagaku (Kyoto)*, 1989, **44**, 570–575.

40. K. Tanaka, *Denki Kagaku Oyobi Kogyo Butsuri Kagaku*, 1990, **58**, 989–996.
41. H. Ishida, T. Terada, K. Tanaka and T. Tanaka, *Inorganic Chemistry*, 1990, **29**, 905–911.
42. H. Ishida, K. Tanaka and T. Tanaka, *Chemistry Letters*, 1988, 339–342.
43. H. Tanaka, H. Nagao, S. M. Peng and K. Tanaka, *Organometallics*, 1992, **11**, 1450–1451.
44. M. R. M. Bruce, E. Megehee, B. P. Sullivan, H. Thorp, T. R. O'Toole, A. Downard and T. J. Meyer, *Organometallics*, 1988, **7**, 238–240.
45. M. R. M. Bruce, E. Megehee, B. P. Sullivan, H. H. Thorp, T. R. O'Toole, A. Downard, J. R. Pugh and T. J. Meyer, *Inorganic Chemistry*, 1992, **31**, 4864–4873.
46. J. R. Pugh, M. R. M. Bruce, B. P. Sullivan and T. J. Meyer, *Inorganic Chemistry*, 1991, **30**, 86–91.
47. N. R. de Tacconi, W. Chanmanee, B. H. Dennis, F. M. MacDonnell, D. J. Boston and K. Rajeshwar, *Electrochem. Solid-State Lett.*, 2012, **15**, B5–B8.
48. N. R. de Tacconi, K. Rajeshwar, W. Chanmanee, V. Valluri, W. A. Wampler, W.-Y. Lin and L. Nikiel, *J. Electrochem. Soc.*, 2010, **157**, B147.
49. N. R. de Tacconi, C. R. Chenthamarakshan, K. Rajeshwar, W.-Y. Lin, T. F. Carlson, L. Nikiel, W. A. Wamper, S. Sambandam and V. Ramani, *J. Electrochem. Soc.*, 2008, **155**, B1102.
50. W. Y. Lin, C. Wei and K. Rajeshwar, *J. Electrochem. Soc.*, 1993, **140**, 2477.
51. A. J. Bard and L. R. Faulkner, *Electrochemical Methods Fundeamentals and Applications*, Second edn., John Wiley & Sons, Inc, New York, New York, 2001.
52. *GSI Chemical Data Base*, http://www.gsi-net.com/en/publications/gsi-chemical-database/single/474.html, Accessed 2012.
53. T. Ikeda, P. Denisevich, K. Willman and R. W. Murray, *J. Am. Chem. Soc.*, 1982, **104**, 2683.
54. Y. Hori, H. Wakebe, T. Tsukamoto and O. Koga, *Electrochimica Acta*, 1994, **39**, 1833.
55. V. Y. Gavrilov and R. S. Zakharov, *Kinetics and Catalysis*, 2010, **51**, 633.
56. N. R. de Tacconi, H. Wenren, D. McChesney and K. Rajeshwar, *Langmuir*, 1998, **14**, 2933.
57. C. Kutal, A. J. Corbin and G. Ferraudi, *Organometallics*, 1987, **6**, 553–557.
58. Y. Hayashi, S. Kita, B. S. Brunschwig and E. Fujita, *J. Am. Chem. Soc.*, 2003, **125**, 11976–11987.
59. C. Kutal, M. A. Weber, G. Ferraudi and D. Geiger, *Organometallics*, 1985, **4**, 2161–2166.
60. H. Takeda and O. Ishitani, *Coord. Chem. Rev.*, 2010, **254**, 346–354.
61. A. Inagaki and M. Akita, *Coord. Chem. Rev.*, 2010, **254**, 1220–1239.

62. H. Hori, Y. Takano, K. Koike and Y. Sasaki, *Inorg. Chem. Commun.*, 2003, **6**, 300–303.
63. J. Hawecker, J. M. Lehn and R. Ziessel, *J. Chem. Soc., Chem. Commun.*, 1985, 56–58.
64. J. Hawecker, J. M. Lehn and R. Ziessel, *J. Chem. Soc., Chem. Commun.*, 1983, 536–538.
65. H. Takeda, K. Koike, H. Inoue and O. Ishitani, *J. Am. Chem. Soc.*, 2008, **130**, 2023–2031.
66. H. Hori, F. P. A. Johnson, K. Koike, O. Ishitani and T. Ibusuki, *J. Photochem. Photobiol., A*, 1996, **96**(171–174).
67. H. Takeda, K. Koike, T. Morimoto, H. Inumaru and O. Ishitani, in *Advances in Inorganic Chemistry*, E. Rudi vanand S. Grażyna, Academic Press, 2011, vol. 63 , pp. 137–186.
68. H. Hori, F. P. A. Johnson, K. Koike, K. Takeuchi, T. Ibusuki and O. Ishitani, *J. Chem. Soc., Dalton Trans.*, 1997, 1019–1023.
69. B. Gholamkhass, H. Mametsuka, K. Koike, T. Tanabe, M. Furue and O. Ishitani, *Inorganic Chemistry*, 2005, **44**, 2326–2336.
70. S. Sato, K. Koike, H. Inoue and O. Ishitani, *Photochem. Photobiol. Sci.*, 2007, **6**, 454–461.
71. Z.-Y. Bian, K. Sumi, M. Furue, S. Sato, K. Koike and O. Ishitani, *Inorganic Chemistry*, 2008, **47**, 10801–10803.
72. Z.-Y. Bian, K. Sumi, M. Furue, S. Sato, K. Koike and O. Ishitani, *Dalton Trans.*, 2009, 983–993.
73. K. Koike, S. Naito, S. Sato, Y. Tamaki and O. Ishitani, *J. Photochem. Photobiol., A*, 2009, **207**, 109–114.
74. Y. Tamaki, K. Watanabe, K. Koike, H. Inoue, T. Morimoto and O. Ishitani, *Faraday Discussions*, 2012, **155**, 115–127.
75. E. Fujita, B. S. Brunschwig, D. Cabelli, M. W. Renner, L. R. Furenlid, T. Ogata, Y. Wada and S. Yanagida, *Stud. Surf. Sci. Catal.*, 1998, **114**, 97–106.
76. C. A. Craig, L. O. Spreer, J. W. Otvos and M. Calvin, *J. Phys. Chem.*, 1990, **94**, 7957–7960.
77. A. H. A. Tinnemans, T. P. M. Koster, D. H. M. W. Thewissen and A. Mackor, Recl, *J. R. Neth. Chem. Soc.*, 1984, **103**(288–295).
78. J. L. Grant, K. Goswami, L. O. Spreer, J. W. Otvos and M. Calvin, *J. Chem. Soc., Dalton Trans.*, 1987, 2105–2109.
79. E. Kimura, S. Wada, M. Shionoya and Y. Okazaki, *Inorganic Chemistry*, 1994, **33**, 770–778.
80. E. Kimura, X. Bu, M. Shionoya, S. Wada and S. Maruyama, *Inorganic Chemistry*, 1992, **31**, 4542–4546.
81. S. Matsuoka, K. Yamamoto, T. Ogata, M. Kusaba, N. Nakashima, E. Fujita and S. Yanagida, *J. Am. Chem. Soc.*, 1993, **115**, 601–609.
82. T. Ogata, Y. Yamamoto, Y. Wada, K. Murakoshi, M. Kusaba, N. Nakashima, A. Ishida, S. Takamuku and S. Yanagida, *J. Phys. Chem*, 1995, **99**, 11916–11922.

83. T. Ogata, S. Yanagida, B. S. Brunschwig and E. Fujita, *J. Am. Chem. Soc.*, 1995, **117**, 6708–6716.
84. D. Behar, T. Dhanasekaran, P. Neta, C. M. Hosten, D. Ejeh, P. Hambright and E. Fujita, *J. Phys. Chem. A*, 1998, **102**, 2870–2877.
85. J. Grodkowski, D. Behar, P. Neta and P. Hambright, *J. Phys. Chem. A*, 1997, **101**, 248–254.
86. D. J. Boston, C. Xu, D. W. Armstrong and F. M. MacDonnell, Manuscript in Preparation.
87. I. Willner, R. Maidan, D. Mandler, H. Duerr, G. Doerr and K. Zengerle, *J. Am. Chem. Soc.*, 1987, **109**, 6080–6086.
88. R. Maidan and I. Willner, *J. Am. Chem. Soc.*, 1986, **108**, 8100–8101.
89. P. V. Klevtsov and R. F. Klevtsova, *J. Struct. Chem.*, 1977, **18**, 339.
90. N. R. de Tacconi, H. K. Timmaji, W. Chanmanee, M. N. Huda, P. Sarker, C. Janaky and K. Rajeshwar, *ChemPhysChem*, 2012, **13**, 2945.
91. K. Rajeshwar, N. R. de Tacconi and H. K. Timmaji, *J. Nano Res.*, 2012, **17**, 185.
92. D. A. Palmer and R. Vaneldik, *Chemical Reviews*, 1983, **83**, 651.
93. CRC *Handbook of Chemistry and Physics*, 82 edn., CRC Press, Boca Raton, FL, 2001–2001.
94. C. R. Chenthamarakshan and K. Rajeshwar, *Electrochem. Commun.*, 2000, **2**, 527.
95. A. Paracchino, V. Laporte, K. Sivula, M. Gratzel and E. Thimsen, *Nature Materials*, 2011, **10**, 456.
96. S. Somasundaram, C. R. Chenthamaraksha, N. R. de Tacconi and K. Rajeshwar, *Int. J. Hydrogen Energy*, 2007, **32**, 4661.
97. A. Paracchino, J. C. Brauer, J.-E. Moser, E. Thimsen and M. Gratzel, *J. Phys. Chem. C*, 2012, **116**, 7341.
98. Y. Zhou and J. A. Switzer, *Mater. Res. Innovations*, 1998, **2**, 1731.
99. A. E. Rakhshani and J. Varghese, *J. Mater. Sci.*, 1988, **23**, 2847.
100. A. E. Rakhshani, A. A. Al-Jassar and J. Varghese, *Thin Solid Films*, 1987, **148**, 191.
101. L. C. Wang, N. R. de Tacconi, C. R. Chenthamarakshan, K. Rajeshwar and M. Tao, *Thin Solid Films*, 2007, **515**, 3090.
102. Y. Zhou and J. A. Switzer, *Scripta Materialia*, 1998, **38**, 1731.
103. E. W. Bohannan, L.-Y. Huang, F. S. Miller, M. G. Shumsky and J. A. Switzer, *Langmuir*, 1999, **15**, 813.
104. C. C. Hu, J. N. Nian and H. Teng, *Sol. Energy Mater. Sol. Cells*, 2008, **92**, 1071.
105. W. Siripala, A. Ivanovskaya, T. F. Jaramillo, S. H. Baeck and E. W. McFarland, *Sol. Energy Mater. Sol. Cells*, 2003, **77**, 229.
106. P. E. de Jongh, D. Vanmaekelbergh and J. J. Kelly, *J. Electrochem. Soc.*, 2000, **147**, 486.
107. Z. Zheng, B. Huang, Z. Wang, M. Guo, X. Qin, X. Zhang, P. Wang and Y. Dai, *J. Phys. Chem. C*, 2009, **113**, 14448.
108. H. Yoneyama, K. Sugimura and S. Kuwabata, *J. Electroanal. Chem.*, 1988, **249**, 143.

109. A. B. Bocarsly, Q. D. Gibson, A. J. Morris, R. P. L'Esperance, Z. M. Detweiler, P. S. Lakkaraju, E. L. Zeitler and T. W. Shaw, *ACS Catalysis*, 2012, **2**, 1684.
110. E. E. Barton, D. M. Rampulla and A. B. Bocarsly, *J. Am. Chem. Soc.*, 2008, **130**, 6342–6344.
111. N. Myung, N. R. de Tacconi and K. Rajeshwar, To be submitted.
112. K. K. Kanazawa and J. G. Gordon, *Analytical Chemistry*, 1985, **57**, 1770.
113. G. Sauerbrey, *Zeitschrift für Physik*, 1959, **155**, 206.
114. G. Seshadri, C. Lin and A. B. Bocarsly, *J. Electroanal. Chem.*, 1994, **372**, 145–150.
115. A. A. Isse, A. Gennaro, E. Vianello and C. Floriani, *J. Mol. Catal.*, 1991, **70**, 197–208.
116. D. J. Pearce and D. Pletcher, *J. Electroanal. Chem. and Interfacial Electrochemistry*, 1986, **197**, 317–330.
117. S.-N. Pun, W.-H. Chung, K.-M. Lam, P. Guo, P.-H. Chan, K.-Y. Wong, C.-M. Che, T.-Y. Chen and S.-M. Peng, *J. Chem. Soc., Dalton Trans.*, 2002, 575–583.
118. J. Costamagna, J. Canales, J. Vargas and G. Ferraudi, *Pure and Applied Chemistry*, 1995, **67**, 1045–1052.
119. S. Sakaki, *J. Am. Chem. Soc.*, 1992, **114**, 2055–2062.
120. M. Beley, J. P. Collin, R. Ruppert and J. P. Sauvage, *J. Am. Chem. Soc.*, 1986, **108**, 7461–7467.
121. M. Beley, J.-P. Collin, R. Ruppert and J.-P. Sauvage, *J. Chem. Soc., Chem. Commun.*, 1984, 1315–1316.
122. A. Rios-Escudero, M. Isaacs, M. Villagran, J. Zagal and J. Costamagna, *J. Argent. Chem. Soc.*, 2004, **92**, 63–71.
123. M. A. Scibioh and V. R. Virayaraghavan, *Bull. Electrochem.*, 1997, **13**, 275–279.
124. M. A. Scihioh and V. R. Virayaraghavan, *Bull. Electrochem.*, 2000, **16**, 376–381.
125. A. C. De, J. A. Crayston, T. Cromie, T. Eisenblatter, R. W. Hay, Y. D. Lampeka and L. V. Tsymbal, *Electrochim. Acta*, 2000, **45**, 2061–2074.
126. I. S. Adaev, T. V. Korostoshevskaya, V. T. Novikov and T. V. Lysyak, *Russ. J. Electrochem.*, 2005, **41**, 1125–1129.
127. T. Atoguchi, A. Aramata, A. Kazusaka and M. Enyo, *J. Chem. Soc., Chem. Commun.*, 1991, 156–157.
128. I. M. B. Nielsen and K. Leung, *J. Phys. Chem. A*, 2010, **114**, 10166–10173.
129. M. Tezuka and M. Iwasaki, *Chemistry Letters*, 1993, 427–430.
130. I. Bhugun, D. Lexa and J.-M. Saveant, *J. Am. Chem. Soc.*, 1996, **118**, 1769–1776.
131. I. Bhugun, D. Lexa and J.-M. Savéant, *J. Am. Chem. Soc.*, 1994, **116**, 5015–5016.
132. I. Bhugun, D. Lexa and J.-M. Savéant, *J. Phys. Chem.*, 1996, **100**, 19981–19985.
133. M. Hammouche, D. Lexa, M. Momenteau and J. M. Saveant, *J. Am. Chem. Soc.*, 1991, **113**, 8455–8466.

134. M. Hammouche, D. Lexa, J. M. Savéant and M. Momenteau, *J. Electroanal. Chem. Interfacial Electrochem.*, 1988, **249**, 347–351.
135. C. Arana, M. Keshavarz, K. T. Potts and H. D. Abruña, *Inorganica Chimica Acta*, 1994, **225**, 285–295.
136. J. A. Ramos Sende, C. R. Arana, L. Hernandez, K. T. Potts, M. Keshevarz-K and H. D. Abruna, *Inorganic Chemistry*, 1995, **34**, 3339–3348.
137. S. Daniele, P. Ugo, G. Bontempelli and M. Fiorani, *J. Electroanal. Chem. Interfacial Electrochem.*, 1987, **219**, 259–271.
138. H. Ishida, K. Tanaka and T. Tanaka, *Organometallics*, 1987, **6**, 181–186.
139. A. I. Breikss and H. D. Abruna, *J. Electroanal. Chem.*, 1986, **201**, 347–358.
140. S. Cosnier, A. Deronzier and J.-C. Moutet, *J. Electroanal. Chem. Interfacial Electrochem.*, 1986, **207**, 315–321.
141. C. M. Bolinger, B. P. Sullivan, D. Conrad, J. A. Gilbert, N. Story and T. J. Meyer, *J. Chem. Soc., Chem. Commun.*, 1985, 796–797.
142. C. M. Bolinger, N. Story, B. P. Sullivan and T. J. Meyer, *Inorganic Chemistry*, 1988, **27**, 4582–4587.
143. K. S. Ratliff, R. E. Lentz and C. P. Kubiak, *Organometallics*, 1992, **11**, 1986–1988.
144. S. Slater and J. H. Wagenknecht, *J. Am. Chem. Soc.*, 1984, **106**, 5367–5368.
145. A. Szymaszek and F. P. Pruchnik, *J. Organomet. Chem.*, 1989, **376**, 133–140.
146. D. L. DuBois and A. Miedaner, *J. Am. Chem. Soc.*, 1987, **109**, 113–117.
147. H. A. G. M. Mostafa, T. Nagaoka and K. Ogura, *Electrochim. Acta*, 1997, **42**, 2577–2585.
148. A. Szymaszek and F. Pruchnik, *Rhodium Express*, 1994, **5**, 18–22.
149. M. Nakazawa, Y. Mizobe, Y. Matsumoto, Y. Uchida, M. Tezuka and M. Hidai, *Bull. Chem. Soc. Jpn.*, 1986, **59**, 809–814.
150. T. Tomohiro, K. Uoto and H. Okuno, *J. Chem. Soc., Chem. Commun.*, 1990, 194–195.
151. J.-M. Lehn and R. Ziessel, *J. Organomet. Chem.*, 1990, **382**, 157–173.
152. N. Kitamura and S. Tazuke, *Chemistry Letters*, 1983, 1109–1112.
153. J.-M. Lehn and R. Ziessel, *Proceedings of the National Academy of Sciences*, 1982, **79**, 701–704.
154. R. Ziessel, J. Hawecker and J.-M. Lehn, *Helv. Chim. Acta*, 1986, **69**, 1065–1084.
155. R. Perutz, C. D. Windle, M. V. Campian, E. Gibson, A. Duhme-Klair and J. Schneider, *Chem. Commun.,* 2012.
156. K. Koike, H. Hori, M. Ishizuka, J. R. Westwell, K. Takeuchi, T. Ibusuki, K. Enjouji, H. Konno, K. Sakamoto and O. Ishitani, *Organometallics*, 1997, **16**, 5724–5729.
157. H. Hori, K. Koike, K. Takeuchi and Y. Sasaki, *Chemistry Letters*, 2000, 522–523.
158. H. Hori, K. Koike, Y. Suzuki, M. Ishizuka, J. Tanaka, K. Takeuchi and Y. Sasaki, *J. Mol. Catal. A: Chem.*, 2002, **179**, 1–9.
159. H. Hori, J. Ishihara, K. Koike, K. Takeuchi, T. Ibusuki and O. Ishitani, *J. Photochem. Photobiol., A*, 1999, **120**, 119–124.